Eur. Phys. J. C 7, 5–27 (1999)
DOI 10.1007/s100529800959

THE EUROPEAN PHYSICAL JOURNAL C

QCD anatomy of $B \to X_s\gamma$ decays

A.L. Kagan[1], M. Neubert[2]

[1] Department of Physics, University of Cincinnati, Cincinnati, Ohio 45221, USA
[2] Theory Division, CERN, CH-1211 Geneva 23, Switzerland

Received: 13 May 1998 / Published online: 3 September 1998

Abstract. We present an updated next-to-leading order analysis of the $B \to X_s\gamma$ branching ratio and photon spectrum, including consistently the effects of Fermi motion in the heavy-quark expansion. For the Standard Model, we obtain $\mathrm{B}(B \to X_s\gamma) = (2.57 \pm 0.26^{+0.31}_{-0.36}) \times 10^{-4}$ for the integral over the high-energy part of the photon spectrum with $E_\gamma^{\rm lab} > 2.2\,\mathrm{GeV}$, where the first error reflects the uncertainty in the input parameters, and the second one the uncertainty in the calculation of Fermi motion. This prediction agrees with the CLEO measurement of the same quantity within one standard deviation. From a reanalysis of the CLEO data, we obtain for the total branching ratio $\mathrm{B}(B \to X_s\gamma) = (2.62 \pm 0.60_{\rm exp}\,{}^{+0.37}_{-0.30\,\rm th}) \times 10^{-4}$ using the measured rate above 2.2 GeV, and $(2.66 \pm 0.56_{\rm exp}\,{}^{+0.43}_{-0.48\,\rm th}) \times 10^{-4}$ using a fit to the photon energy spectrum. Both values are consistent with the Standard Model prediction of $(3.29 \pm 0.33) \times 10^{-4}$. Our analysis contains an improved discussion of renormalization-scale dependence and QED corrections. We also study the sensitivity of the branching ratio and photon spectrum to hadronic parameters such as the b-quark mass, and to possible contributions from New Physics beyond the Standard Model.

1 Introduction

The inclusive radiative decays $B \to X_s\gamma$ have been the subject of a considerable number of experimental and theoretical investigations. About three years ago, the CLEO Collaboration reported a first measurement of the branching ratio for these decays, yielding [1]

$$\mathrm{B}(B \to X_s\gamma) = (2.32 \pm 0.57 \pm 0.35) \times 10^{-4}\,, \qquad (1)$$

where the first error is statistical and the second is systematic (including model dependence). Recently, the ALEPH Collaboration has reported a measurement of the corresponding branching ratio for b-hadrons produced at the Z resonance, yielding [2]

$$\mathrm{B}(H_b \to X_s\gamma) = (3.11 \pm 0.80 \pm 0.72) \times 10^{-4}\,, \qquad (2)$$

which is compatible with the CLEO result.

Being rare processes mediated by loop diagrams, inclusive radiative decays are potentially sensitive probes of New Physics beyond the Standard Model, provided a precise theoretical calculation of the branching ratio can be performed. The general framework for such a calculation is provided by the heavy-quark expansion, which predicts that, up to small bound-state corrections, inclusive decay rates agree with the parton model rates for the underlying decays of the b quark [3–5]. As long as the fine structure of the photon energy spectrum is not probed locally, the theoretical analysis of $B \to X_s\gamma$ decays relies only on the weak assumption of global quark–hadron duality. The leading nonperturbative corrections have been studied in detail and are well understood [6–11]. Still, the theoretical prediction for the branching ratio suffers from large perturbative uncertainties of about 30% if only leading-order expressions for the Wilson coefficient functions in the effective weak Hamiltonian are employed [12–14]. Therefore, it was an important achievement when last year the full next-to-leading order calculation of the total $B \to X_s\gamma$ branching ratio in the Standard Model was completed, combining consistently results for the matching conditions [15,16], matrix elements [17,18] and anomalous dimensions [19]. With this calculation the theoretical uncertainty was reduced to a level of about 10% [19,20]. More recently, the next-to-leading order analysis was also extended to two-Higgs-doublet models [21,22].

Whereas considerable effort has thus gone into calculating the total $B \to X_s\gamma$ branching ratio, little progress has been made in understanding the structure of the photon energy spectrum at next-to-leading order. On the other hand, what is experimentally accessible is only the high-energy part of the photon spectrum, and an understanding of the spectral shape is thus a prerequisite for extrapolating the data to the full phase space. For instance, the CLEO Collaboration has measured the spectrum in the energy range between 2.2 and 2.7 GeV (in the laboratory) and applied a correction factor of 0.87 ± 0.06 to extrapolate to the total decay rate [23][1]. This factor does not take into account the full next-to-leading order corrections to the decay rate. More importantly, it relies on an estimate of bound-state effects [24] obtained using the

[1] A similar treatment is followed in the ALEPH analysis [2]

phenomenological model of Altarelli et al. [25], which is not fully consistent with the heavy-quark expansion. The small uncertainty assigned to the correction factor reflects the fact that the model parameters (the Fermi momentum and the constituent quark masses) have been tuned to fit the lepton spectrum in $B \to X_c\,\ell\,\nu$ decays and then used to predict the photon spectrum in $B \to X_s\gamma$ decays. It is now known that there is no theoretical justification for such a treatment [26–28]. These conceptual shortcomings were not improved in the updated analysis of the photon spectrum presented by Ali and Greub a few years ago [17], although more complete formulae for the perturbative corrections were used in this work and a more conservative error analysis was presented.

The fact that only the high-energy part of the photon spectrum in $B \to X_s\gamma$ decays is accessible experimentally introduces a significant additional theoretical uncertainty [29], which has been ignored in previous analyses. This observation limits the potential of existing data on these decays to probe or constrain New Physics beyond the Standard Model (for recent reviews, see [30,31] and references therein). In this paper, we investigate in a systematic way to what extent the high-energy part of the photon energy spectrum in $B \to X_s\gamma$ decays can be controlled theoretically. The "Fermi motion" of the b quark inside the B meson, which determines the characteristic shape to the photon spectrum, can be consistently described by taking a convolution of the parton model prediction for the spectrum with a universal shape function $F(k_+)$, which determines the light-cone momentum distribution of the b quark in the B meson [26–28]. We will for the first time present a discussion of Fermi motion effects in a full next-to-leading order analysis of $B \to X_s\gamma$ decays. In addition, our analysis contains several improvements over previous works concerning, in particular, the estimate of perturbative uncertainties, and the inclusion of QED corrections. In Sect. 2, we discuss in detail the structure of the $B \to X_s\gamma$ branching ratio at next-to-leading order in QCD, correcting some errors in the formulae for real-gluon radiation contributions employed by previous authors. We introduce a decomposition of the branching ratio in terms of the values of the Wilson coefficients $C_i(m_W)$ at the weak scale, which is particularly convenient to discuss the sensitivity to New Physics beyond the Standard Model. This decomposition is also the starting point of a thorough discussion of the renormalization-scale dependence. We find that the perturbative uncertainty in the theoretical prediction for the branching ratio has been underestimated by previous authors [19–22] by more than a factor of 2. We also suggest a new definition of the "total" branching ratio, which is insensitive to the unphysical soft-photon divergence in the $b \to sg\gamma$ subprocess. In Sect. 3, we show that Fermi motion effects, which result from the residual interaction of the b quark inside the B meson, give rise to the dominant theoretical uncertainty in the calculation of the partially integrated (over photon energy) branching ratio. We present a consistent treatment of these effects based on first principles of the heavy-quark expansion, emphasizing that for such partially integrated quantities the main element of uncertainty in the description of Fermi motion lies in the value of the b-quark mass. Other features associated with the detailed functional form of the shape function play a minor role. We make a prediction for the $B \to X_s\gamma$ branching ratio with a restriction on the photon energy such that $E_\gamma^{\rm lab} > 2.2\,{\rm GeV}$ and find agreement with the CLEO measurement of the same quantity within one standard deviation. We also extract a new value for the total branching ratio, which is significantly different from the published CLEO result reported in (1). In Sect. 4, we extend the discussion to the photon spectrum itself, investigating first the structure of the contributions from different operators in the effective Hamiltonian. We find that, to a high degree of accuracy, the shape of the photon spectrum is determined by QCD dynamics and is insensitive to New Physics beyond the Standard Model. We then perform a fit of our theoretical predictions to the CLEO data on the photon spectrum and extract again a value for the total branching ratio. We also discuss the possibility of determining, from future high-precision data on the photon spectrum, a value of the b-quark mass with a well-defined short-distance interpretation. In Sect. 5, we consider the hadronic invariant mass spectrum and discuss the role of quark–hadron duality in the comparison of experimental data with our theoretical predictions. We derive a realistic, one-parameter description of the spectrum that is valid even in the low-mass region, where quark–hadron duality breaks down. Finally, in Sect. 6 we explore how New Physics beyond the Standard Model may affect the spectral shape and the total branching ratio in $B \to X_s\gamma$ decays. Section 7 contains the conclusions. The paper also comprises three Appendices, where we discuss QED corrections to the $B \to X_s\gamma$ branching ratio, the Doppler broadening of the photon spectrum in the decays of B mesons produced at the $\Upsilon(4s)$ resonance, and technical details of the calculation of the photon energy spectrum.

2 $B \to X_s\gamma$ branching ratio

The theoretical analysis of the $B \to X_s\gamma$ branching ratio at next-to-leading order has been discussed previously by several authors. In this section we review the main ingredients of the calculation. In addition, we present several improvements of it, which concern the treatment of leading-logarithmic QED corrections, the analysis of the renormalization-scale dependence, and a discussion of the sensitivity to New Physics. We also correct some mistakes in the results for real-gluon emission presented in the literature.

The starting point in the calculation of inclusive B decay rates is the low-energy effective Hamiltonian [32]

$$H_{\rm eff} = -\frac{4G_F}{\sqrt{2}}\,V_{ts}^*V_{tb}\sum_i C_i(\mu_b)O_i(\mu_b)\,. \tag{3}$$

The operators relevant to our discussion are

$$O_2 = \bar s_L\gamma_\mu c_L\bar c_L\gamma^\mu b_L\,, \quad O_7 = \frac{e\,m_b}{16\pi^2}\,\bar s_L\sigma_{\mu\nu}F^{\mu\nu}b_R\,,$$

$$O_8 = \frac{g_s m_b}{16\pi^2}\,\bar s_L \sigma_{\mu\nu} G_a^{\mu\nu} t_a b_R\,. \tag{4}$$

To an excellent approximation, the contributions of other operators can be neglected. The renormalization scale μ_b in (3) is conveniently chosen of order m_b, so that all large logarithms reside in the Wilson coefficient functions. The complete theoretical prediction for the $B \to X_s\gamma$ decay rate at next-to-leading order has been presented for the first time by Chetyrkin et al. [19]. It depends on a parameter δ defined by the condition that the photon energy be above a threshold given by $E_\gamma > (1-\delta)E_\gamma^{\max}$, where $E_\gamma^{\max} = m_b/2$ is the maximum photon energy attainable in the parton model. (Throughout this paper, we will neglect the mass of the strange quark whenever possible.) The prediction for the $B \to X_s\gamma$ branching ratio is usually obtained by normalizing the result for the corresponding decay rate to that for the semileptonic decay rate, thereby eliminating a strong dependence on the b-quark mass. We define

$$\begin{aligned} R_{\rm th}(\delta) &= \frac{\Gamma(B\to X_s\gamma)\big|_{E_\gamma>(1-\delta)E_\gamma^{\max}}}{\Gamma(B\to X_c\,e\,\bar\nu)} \\ &= \frac{6\alpha}{\pi f(z)}\left|\frac{V_{ts}^* V_{tb}}{V_{cb}}\right|^2 K_{\rm NLO}(\delta)\,, \end{aligned} \tag{5}$$

where $f(z) = 1 - 8z + 8z^3 - z^4 - 12z^2\ln z \approx 0.542 - 2.23(\sqrt{z} - 0.29)$ is a phase-space factor depending on the mass ratio $z = (m_c/m_b)^2$, for which we shall take $\sqrt{z} = 0.29 \pm 0.02$. In the context of our analysis, the quark masses are defined as one-loop pole masses. The electromagnetic coupling $\alpha = 1/137.036$ is the fine-structure constant renormalized at $q^2 = 0$, as is appropriate for real-photon emission [33]. The quantity $K_{\rm NLO}(\delta) = |C_7|^2 + \ldots$ contains the corrections to the leading-order result. In terms of the theoretically calculable ratio $R_{\rm th}(\delta)$, the $B \to X_s\gamma$ branching ratio is given by

$$\begin{aligned} {\rm B}(B\to X_s\gamma)\big|_{E_\gamma>(1-\delta)E_\gamma^{\max}} &= R_{\rm th}(\delta)\times {\rm B}(B\to X_c\,e\,\bar\nu) \\ &= 0.105 N_{\rm SL}\, R_{\rm th}(\delta)\,, \end{aligned} \tag{6}$$

where $N_{\rm SL} = {\rm B}(B \to X_c\,e\,\bar\nu)/10.5\%$ is a normalization factor to be determined from experiment. To good approximation $N_{\rm SL} = 1$. The current experimental situation of measurements of the semileptonic branching ratio of B mesons and their theoretical interpretation are reviewed in [34,35].

In the calculation of the quantity $K_{\rm NLO}(\delta)$ we shall consistently work to first order in the small parameters α_s, $1/m_Q^2$ and α/α_s, the latter ratio being related to the leading-logarithmic QED corrections. The general structure of the result is

$$\begin{aligned} K_{\rm NLO}(\delta) = &\sum_{\substack{i,j=2,7,8\\ i\le j}} k_{ij}(\delta,\mu_b)\,{\rm Re}\Big[C_i^{(0)}(\mu_b)\,C_j^{(0)*}(\mu_b)\Big] \\ &+S(\delta)\,\frac{\alpha_s(\mu_b)}{2\pi}\,{\rm Re}\Big[C_7^{(1)}(\mu_b)\,C_7^{(0)*}(\mu_b)\Big] \\ &+S(\delta)\,\frac{\alpha}{\alpha_s(\mu_b)}\bigg(2\,{\rm Re}\Big[C_7^{(\rm em)}(\mu_b)\,C_7^{(0)*}(\mu_b)\Big] \\ &-k_{\rm SL}^{(\rm em)}(\mu_b)\,|C_7^{(0)}(\mu_b)|^2\bigg)\,, \end{aligned} \tag{7}$$

where we have expanded the Wilson coefficients as[2]

$$\begin{aligned} C_i(\mu_b) = C_i^{(0)}(\mu_b) &+ \frac{\alpha_s(\mu_b)}{4\pi}\,C_i^{(1)}(\mu_b) \\ &+\frac{\alpha}{\alpha_s(\mu_b)}\,C_i^{(\rm em)}(\mu_b) + \ldots\,. \end{aligned} \tag{8}$$

The leading-order coefficients are given by

$$\begin{aligned} C_2^{(0)}(\mu_b) &= \frac{1}{2}\left(\eta^{-\frac{12}{23}} + \eta^{\frac{6}{23}}\right), \\ C_7^{(0)}(\mu_b) &= \eta^{\frac{16}{23}}\,C_7^{(0)}(m_W) \\ &\quad +\frac{8}{3}\left(\eta^{\frac{14}{23}} - \eta^{\frac{16}{23}}\right)C_8^{(0)}(m_W) + \sum_{i=1}^{8} h_i\,\eta^{a_i}\,, \\ C_8^{(0)}(\mu_b) &= \eta^{\frac{14}{23}}\,C_8^{(0)}(m_W) + \sum_{i=1}^{8} \bar h_i\,\eta^{a_i}\,, \end{aligned} \tag{9}$$

where $\eta = \alpha_s(m_W)/\alpha_s(\mu_b)$, and h_i, $\bar h_i$ and a_i are known numerical coefficients [13,14]. In the Standard Model, the Wilson coefficients of the dipole operators at the scale m_W are functions of the mass ratio $x_t = (\overline{m}_t(m_W)/m_W)^2$ given by [12]

$$\begin{aligned} C_7^{(0)}(m_W) &= \frac{3x_t^3 - 2x_t^2}{4(x_t-1)^4}\ln x_t + \frac{-8x_t^3 - 5x_t^2 + 7x_t}{24(x_t-1)^3}\,, \\ C_8^{(0)}(m_W) &= \frac{-3x_t^2}{4(x_t-1)^4}\ln x_t + \frac{-x_t^3 + 5x_t^2 + 2x_t}{8(x_t-1)^3}\,. \end{aligned} \tag{10}$$

The next-to-leading terms in (8) must be kept only for the coefficient $C_7(\mu_b)$. The expression for $C_7^{(1)}(\mu_b)$ can be found in (21) of [19]. Our treatment of QED corrections differs from that of Czarnecki and Marciano [33] in that we perform a renormalization-group improvement to resum the contributions to $C_7(\mu_b)$ of order $\alpha L\,(\alpha_s L)^n$, with $L = \ln(m_W/\mu_b)$, to all orders in perturbation theory, whereas these authors include only the terms with $n = 0$. Numerically, the resummation decreases the effect of QED correction by almost a factor of 2. The technical details of our calculation are discussed in Appendix A. The result for $C_7^{(\rm em)}(\mu_b)$ is

$$\begin{aligned} C_7^{(\rm em)}(\mu_b) = &\left(\frac{32}{75}\,\eta^{-\frac{9}{23}} - \frac{40}{69}\,\eta^{-\frac{7}{23}} + \frac{88}{575}\,\eta^{\frac{16}{23}}\right)C_7^{(0)}(m_W) \\ &+\left(-\frac{32}{575}\,\eta^{-\frac{9}{23}} + \frac{32}{1449}\,\eta^{-\frac{7}{23}} + \frac{640}{1449}\,\eta^{\frac{14}{23}}\right. \\ &\left.-\frac{704}{1725}\,\eta^{\frac{16}{23}}\right)C_8^{(0)}(m_W) - \frac{190}{8073}\,\eta^{-\frac{35}{23}} \\ &-\frac{359}{3105}\,\eta^{-\frac{17}{23}} + \frac{4276}{121095}\,\eta^{-\frac{12}{23}} + \frac{350531}{1009125}\,\eta^{-\frac{9}{23}} \\ &+\frac{2}{4347}\,\eta^{-\frac{7}{23}} - \frac{5956}{15525}\,\eta^{\frac{6}{23}} + \frac{38380}{169533}\,\eta^{\frac{14}{23}} \\ &-\frac{748}{8625}\,\eta^{\frac{16}{23}}\,. \end{aligned} \tag{11}$$

[2] These are the effective, scheme-independent Wilson coefficient functions introduced in [14]

The result for the leading QED correction to the semileptonic decay rate is [36]

$$k_{\rm SL}^{(\rm em)}(\mu_b) = \frac{12}{23}\left(\eta^{-1}-1\right) \simeq \frac{2\alpha_s(\mu_b)}{\pi}\ln\frac{m_W}{\mu_b}\,. \qquad (12)$$

We note that unlike the factor α in (5), which results from the calculation of a matrix element for a process with real-photon emission, the QED corrections to the Wilson coefficients arise from the evolution of local operators, and hence the coupling α in (8) should in principle be taken as a running coupling $\alpha(\mu)$ rather than the fine-structure constant renormalized at $q^2=0$. However, including the running of the QED coupling in the operator evolution would only induce corrections of order $(\alpha L)^2(\alpha_s L)^n$, which from a numerical point of view can be safely neglected.

For the purpose of illustration, we note that with $\mu_b = 4.8\,\text{GeV}$ the values of the various coefficients in the Standard Model are: $C_2^{(0)}(m_b) \approx 1.11$, $C_7^{(0)}(m_b) \approx -0.31$, $C_8^{(0)}(m_b) \approx -0.15$, as well as $C_7^{(1)}(m_b) \approx 0.48$ and $C_7^{(\rm em)}(m_b) \approx 0.03$. The QED correction proportional to $C_7^{(\rm em)}$ in (7) is about a factor 0.13 smaller than the next-to-leading order QCD correction proportional to $C_7^{(1)}$.

The coefficient functions $k_{ij}(\delta,\mu_b)$ in (7) are given by

$$\begin{aligned}
k_{77}(\delta,\mu_b) &= S(\delta)\left\{1+\frac{\alpha_s(\mu_b)}{2\pi}\left(r_7+\gamma_{77}\ln\frac{m_b}{\mu_b}-\frac{16}{3}\right)\right.\\
&\quad\left.+\left[\frac{(1-z)^4}{f(z)}-1\right]\frac{6\lambda_2}{m_b^2}\right\}\\
&\quad+\frac{\alpha_s(\mu_b)}{\pi}\,f_{77}(\delta)+S(\delta)\,\frac{\alpha_s(\bar\mu_b)}{2\pi}\,\bar\kappa(z)\,,\\
k_{27}(\delta,\mu_b) &= S(\delta)\left[\frac{\alpha_s(\mu_b)}{2\pi}\left(\mathrm{Re}(r_2)+\gamma_{27}\ln\frac{m_b}{\mu_b}\right)-\frac{\lambda_2}{9m_c^2}\right]\\
&\quad+\frac{\alpha_s(\mu_b)}{\pi}\,f_{27}(\delta)\,,\\
k_{78}(\delta,\mu_b) &= S(\delta)\,\frac{\alpha_s(\mu_b)}{2\pi}\left(\mathrm{Re}(r_8)+\gamma_{87}\ln\frac{m_b}{\mu_b}\right)\\
&\quad+\frac{\alpha_s(\mu_b)}{\pi}\,f_{78}(\delta)\,,\\
k_{ij}(\delta,\mu_b) &= \frac{\alpha_s(\mu_b)}{\pi}\,f_{ij}(\delta)\,;\\
\{i,j\} &= \{2,2\},\,\{8,8\},\,\{2,8\}\,, \qquad (13)
\end{aligned}$$

where

$$S(\delta) = \exp\left[-\frac{2\alpha_s(\mu_b)}{3\pi}\left(\ln^2\delta+\frac{7}{2}\ln\delta\right)\right] \qquad (14)$$

is a Sudakov factor, $\gamma_{77}=\frac{32}{3}$, $\gamma_{27}=\frac{416}{81}$ and $\gamma_{87}=-\frac{32}{9}$ are entries of the anomalous dimension matrix, and

$$\begin{aligned}
r_7 &= -\frac{10}{3}-\frac{8\pi^2}{9}\,, \qquad \mathrm{Re}(r_8) = \frac{44}{9}-\frac{8\pi^2}{27}\,,\\
\mathrm{Re}(r_2) &\approx -4.092+12.78(\sqrt{z}-0.29) \qquad (15)
\end{aligned}$$

are numerical coefficients resulting from the calculation of the matrix elements of the local operators O_i in the effective Hamiltonian at next-to-leading order [18]. Finally, $\bar\kappa(z) \approx 3.382-4.14(\sqrt{z}-0.29)$ is the next-to-leading correction to the semileptonic decay rate [37]. To $O(\alpha_s)$ the explicit μ_b dependence of the coefficients $k_{ij}(\delta,\mu_b)$ cancels against that of the Wilson coefficient functions. Following [20], we allow for different renormalization scales in radiative and semileptonic B decays (i.e. $\mu_b \neq \bar\mu_b$).

The functions $f_{ij}(\delta)$ in (13) account for the effects of real-gluon radiation and are defined such that $f_{ij}(0)=0$. They can be obtained from results given in [17,18] by performing some phase-space integrations. We find

$$\begin{aligned}
f_{77}(\delta) &= \frac{1}{3}\left[10\delta+\delta^2-\frac{2\delta^3}{3}+\delta(\delta-4)\ln\delta\right],\\
f_{88}(\delta) &= \frac{1}{27}\left\{4L_2(1-\delta)-\frac{2\pi^2}{3}+8\ln(1-\delta)\right.\\
&\quad -\delta(2+\delta)\ln\delta+7\delta+3\delta^2-\frac{2\delta^3}{3}\\
&\quad\left.-2\left[2\delta+\delta^2+4\ln(1-\delta)\right]\ln\frac{m_b}{m_s}\right\},\\
f_{78}(\delta) &= \frac{8}{9}\left[L_2(1-\delta)-\frac{\pi^2}{6}-\delta\ln\delta+\frac{9\delta}{4}-\frac{\delta^2}{4}+\frac{\delta^3}{12}\right],\\
f_{22}(\delta) &= \frac{16}{27}\int_0^1 \mathrm{d}x\,(1-x)(1-x_\delta)\left|\frac{z}{x}\,G\Big(\frac{x}{z}\Big)+\frac{1}{2}\right|^2,\\
f_{27}(\delta) &= -3f_{28}(\delta)\\
&= -\frac{8z}{9}\int_0^1 \mathrm{d}x\,(1-x_\delta)\,\mathrm{Re}\Big[G\Big(\frac{x}{z}\Big)+\frac{x}{2z}\Big]\,, \qquad (16)
\end{aligned}$$

where $x_\delta = \max(x,1-\delta)$, and

$$G(t) = \begin{cases} -2\arctan^2\sqrt{t/(4-t)} & ;\ t<4\,,\\ 2\left(\ln\left[(\sqrt{t}+\sqrt{t-4})/2\right]-\dfrac{i\pi}{2}\right)^2 & ;\ t\geq 4\,. \end{cases} \qquad (17)$$

Our expressions for $f_{78}(\delta)$ and $f_{88}(\delta)$ disagree with the corresponding ones in [19], which have later been used by several authors. (The corrected expressions are also given in an Erratum to [19].) We shall comment on the numerical effect of this correction below. The function f_{88} is sensitive to collinear singularities regulated by the mass of the strange quark. The collinear logarithms can be resummed to all orders of perturbation theory, leading to a collinear-safe result [38]. Unless δ is chosen very close to 1, the net effect of the resummation is a moderate increase of the result. Since the contribution proportional to f_{88} is very small, however, it is sufficient for all practical purposes to work with the leading-order expression given above. We take a rather large value for the quark-mass ratio, $m_b/m_s = 50$, in order to mimic the effect of the resummation of collinear logarithms.

Bound-state corrections enter the theoretical expressions for the coefficients k_{ij} at order $1/m_Q^2$ and are proportional to the hadronic parameter $\lambda_2 = \frac{1}{4}(m_{B^*}^2-m_B^2) \approx$

$0.12\,\text{GeV}^2$ [39]. The corrections proportional to $1/m_b^2$ entering the expression for k_{77} characterize a spin-dependent interaction inside the B meson [4–6]. A peculiar feature of inclusive radiative decays is the appearance of the correction proportional to $1/m_c^2$ in k_{27}, which represents a long-distance contribution arising from $(c\bar{c})$ intermediate states [7,8]. Strictly speaking, these effects are non-local in nature; however, to a good approximation they can be represented by a local $1/m_c^2$ correction [9,10]. The correct sign of this term has only recently been found in [11].

Finally, a comment is in order about our treatment of the Sudakov factor, which is slightly different from that of previous authors. In [19–21], the Sudakov factor was only included for the leading term in k_{77}. If this is done, the decay rate becomes negative for small values of δ, which is an unphysical result. All terms not vanishing in the limit $\delta = 0$ correspond to a two-body decay $b \to s\gamma$ and must be suppressed by a Sudakov factor. Once this is done, the quantity $K_{\rm NLO}(\delta)$ vanishes in the limit $\delta \to 0$ as it should. A full next-to-leading order resummation of Sudakov logarithms that goes beyond the naive exponentiation of the one-loop result shown in (14) is possible but rather complicated. In [40,41], such a resummation has been performed for high-order moments of the photon energy spectrum; however, the results are such that a numerical evaluation would require integration over the running coupling constant $\alpha_s(k_\perp)$ in the region $\Lambda_{\rm QCD} < k_\perp < m_b$. In [42], the resummation has been extended to the partially integrated photon spectrum itself (rather than its moments), and a factorization of short- and long-distance contributions has been performed such that all contributions from scales $k_\perp$ in the range $(\Lambda_{\rm QCD} m_b)^{1/2} < k_\perp < m_b$ are treated perturbatively, whereas contributions from scales in the range $\Lambda_{\rm QCD} < k_\perp < (\Lambda_{\rm QCD} m_b)^{1/2}$ are absorbed into the definition of the shape function. This guarantees that the resummed formulae can be reliably evaluated in perturbation theory. If this is done, it turns out that the resummation is a very small effect, which can be neglected for all practical purposes [42].

In order to explore the sensitivity of the theoretical prediction for the $B \to X_s\gamma$ branching ratio to possible New Physics contributions, it is instructive to make explicit the dependence of the result on the values of the Wilson coefficients of the dipole operators O_7 and O_8 at the scale m_W. To this end, we introduce the ratios

$$\xi_7 = \frac{C_7(m_W)}{C_7^{\rm SM}(m_W)}\,, \qquad \xi_8 = \frac{C_8(m_W)}{C_8^{\rm SM}(m_W)}\,. \tag{18}$$

They are normalized to the Standard Model contributions, which at next-to-leading order take the values $C_7^{\rm SM}(m_W) \approx -0.22$ and $C_8^{\rm SM}(m_W) \approx -0.12$ [15,16]. In many extensions of the Standard Model there are contributions to $C_7(m_W)$ and $C_8(m_W)$ from new flavour physics at a high scale, and consequently the parameters ξ_7 and ξ_8 may take (even complex) values different from 1. Similarly, New Physics may induce dipole operators with opposite chirality to that of the Standard Model, i.e. operators with right-handed light-quark fields. If we denote by C_7^R and C_8^R the Wilson coefficients of these new operators, the expression (7) can be modified to include their contributions by simply replacing $C_i C_j^* \to C_i C_j^* + C_i^R C_j^{R*}$ everywhere, taking however into account that $C_2^R = 0$. We thus define two additional parameters

$$\xi_7^R = \frac{C_7^R(m_W)}{C_7^{\rm SM}(m_W)}\,, \qquad \xi_8^R = \frac{C_8^R(m_W)}{C_8^{\rm SM}(m_W)}\,, \tag{19}$$

which vanish in the Standard Model. Since the dipole operators only contribute to rare flavour-changing neutral current processes, there are at present rather weak constraints on the values of these parameters (see Sect. 6). On the other hand, we assume that the coefficient C_2 of the current–current operator O_2 takes its Standard Model value, and that there is no similar operator containing right-handed quark fields. Since the operator O_2 mediates Cabibbo-allowed decays of B mesons, any significant New Physics contribution to C_2 would already have been detected experimentally.

With these definitions, the $B \to X_s\gamma$ branching ratio can be decomposed as

$$\begin{aligned}
&\frac{1}{N_{\rm SL}}\,\text{B}(B \to X_s\gamma)\big|_{E_\gamma > (1-\delta)E_\gamma^{\rm max}} \\
&= B_{22}(\delta) + B_{77}(\delta)\left(|\xi_7|^2 + |\xi_7^R|^2\right) + B_{88}(\delta)\left(|\xi_8|^2 + |\xi_8^R|^2\right) \\
&\quad + B_{27}(\delta)\,\text{Re}(\xi_7) + B_{28}(\delta)\,\text{Re}(\xi_8) \\
&\quad + B_{78}(\delta)\left[\text{Re}(\xi_7\xi_8^*) + \text{Re}(\xi_7^R\xi_8^{R*})\right]\,.
\end{aligned} \tag{20}$$

The components $B_{ij}(\delta)$ are formally independent of the renormalization scale μ_b. Their residual scale dependence results only from the truncation of perturbation theory at next-to-leading order. In Table 1, the values of these quantities are given for different choices of the renormalization scale and the cutoff on the photon energy. The input parameters entering the calculation will be discussed below. Typically, the components B_{ij} vary by amounts of order 10–20% as μ_b varies between $m_b/2$ and $2m_b$. The good stability is a result of the explicit cancelation of the μ_b dependence between the Wilson coefficients and matrix elements achieved by a full next-to-leading order calculation. The Standard Model branching ratio is obtained by adding the various contributions setting $\xi_7 = \xi_8 = 1$ and $\xi_7^R = \xi_8^R = 0$, as shown in the last column. The most important contributions are the 2-2 and 2-7 terms, followed by the 7-7 term. Note that with a realistic choice of the cutoff parameter δ the coefficient $B_{88}(\delta)$ of the term proportional to $|\xi_8|^2 + |\xi_8^R|^2$ is very small. Therefore, $B \to X_s\gamma$ decays have a low sensitivity to enhanced chromo-magnetic dipole transitions. For the remainder of this section we focus on the Standard Model and evaluate the various theoretical uncertainties in the prediction for the branching ratio. The impact of New Physics will be discussed in Sect. 6.

In Table 1, the choice $\delta = 0.9$ corresponds to the unrealistic case of an almost fully inclusive measurement, whereas $\delta = 0.3$ and 0.15 correspond to a restriction to the high-energy part of the photon spectrum, which in practice is required for experimental reasons. The theoretical

Table 1. Values of the coefficients $B_{ij}(\delta)$ in units of 10^{-4}, for different choices of μ_b

μ_b	δ	B_{22}	B_{77}	B_{88}	B_{27}	B_{28}	B_{78}	$\sum B_{ij}$
$m_b/2$	0.90	1.321	0.335	0.015	1.265	0.179	0.074	3.188
	0.30	1.167	0.322	0.005	1.196	0.136	0.070	2.896
	0.15	1.080	0.309	0.004	1.143	0.126	0.067	2.728
m_b	0.90	1.258	0.382	0.015	1.395	0.161	0.083	3.293
	0.30	1.239	0.361	0.005	1.387	0.137	0.080	3.210
	0.15	1.200	0.347	0.004	1.354	0.132	0.077	3.114
$2m_b$	0.90	1.023	0.428	0.015	1.517	0.132	0.092	3.206
	0.30	1.041	0.402	0.004	1.552	0.118	0.091	3.209
	0.15	1.021	0.386	0.004	1.535	0.115	0.088	3.150

Table 2. Different sources of theoretical uncertainties (in%)

δ	μ_b	$\bar\mu_b$	m_c/m_b	m_b	m_t	$\alpha_s(m_Z)$	CKM	EW cor.	total
0.90	±6.3	$^{+2.2}_{-1.5}$	$^{+5.9}_{-5.0}$	$^{-1.0}_{+1.1}$	$^{+1.6}_{-1.7}$	$^{+2.8}_{-2.7}$	±2.1	±2.0	$^{+10.0}_{-\ 9.3}$
0.30	±6.6	$^{+2.2}_{-1.5}$	$^{+5.5}_{-4.6}$	$^{-1.0}_{+1.0}$	$^{+1.7}_{-1.7}$	$^{+2.6}_{-2.6}$	±2.1	±2.0	$^{+9.9}_{-9.3}$
0.15	±7.1	$^{+2.2}_{-1.5}$	$^{+5.3}_{-4.5}$	$^{-0.9}_{+1.0}$	$^{+1.6}_{-1.7}$	$^{+2.5}_{-2.4}$	±2.1	±2.0	$^{+10.1}_{-\ 9.5}$

prediction for the branching ratio diverges in the limit $\delta \to 1$ because of a logarithmic singularity in the term proportional to $f_{88}(\delta)$, which reflects the soft-photon divergence of the $b \to sg\gamma$ subprocess. Previous authors [19–21] have chosen to define the "total" $B \to X_s\gamma$ branching ratio by taking $\delta = 0.99$. In our opinion this is not the best definition possible, because for values of δ so close to 1 the theoretical result becomes very sensitive to the unphysical soft-photon divergence. This is evident from Fig. 1, which shows the integrated branching ratio as a function of δ. We believe a more reasonable definition of the "total" branching ratio is to use an extrapolation to $\delta = 1$ starting from the region $\delta \sim 0.5$–0.8, where the theoretical result exhibits a weak, almost linear dependence on the cutoff. The simple geometric construction indicated by the dashed lines in the figure shows that the extrapolated value so defined agrees, to a good approximation, with the result obtained by taking $\delta = 0.9$. Hence, from now on we define the "total" branching ratio to be that corresponding to this particular value of the cutoff.

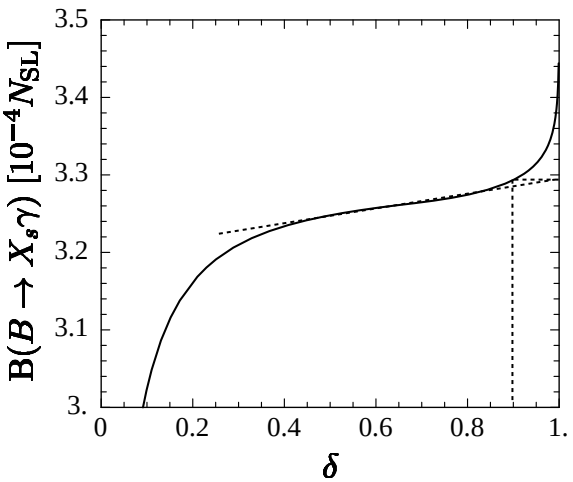

Fig. 1. Dependence of the $B \to X_s\gamma$ branching ratio on the cutoff parameter δ. The dashed lines indicate the extrapolation to the "total" branching ratio

The dependence of the theoretical results on the choice of the renormalization scale is conventionally taken as an estimate of higher-order corrections. Following common practice, we vary the renormalization scales μ_b and $\bar\mu_b$ independently in the range between $m_b/2$ and $2m_b$; their central values are taken to be m_b. The dependence on the scale $\bar\mu_b$ entering the formula for the semileptonic decay rate is straightforward to analyse. The result is shown in Table 2. The analysis of the scale dependence of the radiative decay rate is more subtle. Previous authors have estimated the μ_b dependence of the total branching ratio in the Standard Model and found a striking improvement over the leading-order result. A dedicated discussion of this issue has been presented by Buras et al. [20], and the results obtained in this work were later confirmed in [21,22]. One finds a variation of the total branching ratio by $^{+0.1}_{-3.2}\%$, as compared with $^{+27.4}_{-20.4}\%$ at leading order. We agree with those results, but we believe they cannot be taken as a realistic estimate of the size of unknown higher-order corrections. The excellent stability observed at next-to-leading order is largely due to an accidental cancelation between different contributions to the decay rate. This point of view is supported by the fact that in some extensions of the Standard Model, such as two-Higgs-doublet models, a much stronger scale dependence

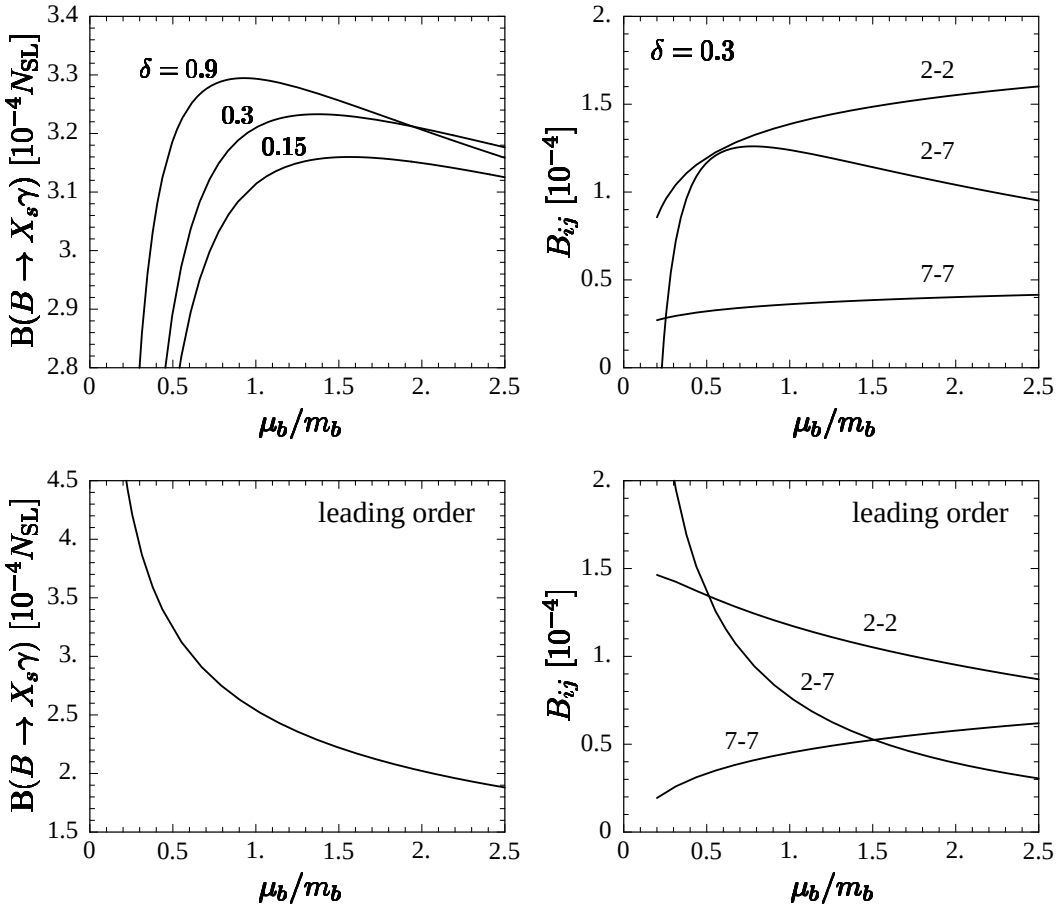

Fig. 2. Scale dependence of the $B \to X_s\gamma$ branching ratio (left) and of its three most important components (right) in the Standard Model. For comparison, the lower plots show the results obtained at leading order

is observed in some regions of parameter space [22]. On the left-hand side in Fig. 2, we show the branching ratio as a function of μ_b/m_b, both at leading and at next-to-leading order. The leading-order result is obtained by replacing the quantity $K_{\rm NLO}(\delta)$ with $|C_7^{(0)}(\mu_b)|^2$. The three curves in the upper plot refer to different choices of δ (there is no cutoff dependence of the leading-order result). Note the different scales in the two plots. The improvement in going from the leading to the next-to-leading order is spectacular and reduces the apparent scale dependence by more than a factor of 10. However, a more careful look at the upper plot reveals two surprises: first, the scale dependence increases rapidly as μ_b is taken below $0.7m_b$, although perturbation theory should work well for lower scales than that; secondly, for $\mu_b > 2m_b$ the prediction for the partially integrated branching ratio with $\delta = 0.3$ exceeds the prediction for the total branching ratio (obtained with $\delta = 0.9$), which is an unphysical result. Both observations indicate that higher-order corrections may be more important than what is suggested by the apparent weak scale dependence of the curves in the plateau region. The scale dependence of the three most important contributions to the branching ratio (those from B_{22}, B_{27} and B_{77}) is illustrated in the right-hand plots in Fig. 2. There is again a significant improvement in going from the leading to the next-to-leading order. However, the residual scale dependence of the quantities B_{ij} at next-to-leading order is much larger than that of their sum, which determines the total branching ratio in the Standard Model. Note, in particular, the almost perfect cancelation of the scale dependence between the 2-2 and the 2-7 term, which is accidental since the magnitude of the 2-7 term depends on the top-quark mass through the value of $C_7^{(0)}(m_W)$ in (10), whereas the 2-2 term is independent of m_t. In such a situation, the apparent weak scale dependence of the sum of all contributions is not a good measure of higher-order corrections. Indeed, higher-order corrections must stabilize the different curves in the right-hand upper plot individually, not only their sum. The variation of the individual components B_{ij} as a function of μ_b thus provides a more conservative estimate of the truncation error than does the variation of the total branching ratio. For each component, we estimate the truncation error by taking one half of the maximum variation obtained by varying μ_b between $m_b/2$ and $2m_b$. The truncation error of the sum is then obtained by adding the individual errors in quadra-

ture. As shown in Table 2, we find a total truncation error of about $\pm 7\%$, which is more than a factor of 2 larger than the estimates obtained by previous authors [19–22]. In our opinion an even larger truncation error could be justified given that the choice of the range of variation of μ_b is ad hoc, and that the scale dependence of the various curves in Fig. 2 is not symmetric around the point $\mu_b = m_b$.

Let us finally discuss the sensitivity of the theoretical prediction for the $B \to X_s\gamma$ branching ratio to the various input parameters entering the calculation. For the quark pole masses, we take $\sqrt{z} = m_c/m_b = 0.29 \pm 0.02$, $m_b = (4.80 \pm 0.15)\,\text{GeV}$, and $m_t = (175 \pm 6)\,\text{GeV}$ corresponding to the running mass $\overline{m}_t(m_W) = (178 \pm 6)\,\text{GeV}$. We use the two-loop expression for the running coupling $\alpha_s(\mu)$ with the initial value $\alpha_s(m_Z) = 0.118 \pm 0.003$. Finally, for the ratio of the CKM parameters we take the value $|V_{ts}^* V_{tb}|/|V_{cb}| = 0.976 \pm 0.010$ obtained from a global analysis of the unitarity triangle [43]. We also include an uncertainty of $\pm 2\%$ to account for next-to-leading electroweak radiative corrections [33]. The theoretical uncertainties arising from the variation of each input parameter are collected in Table 2. Adding the different errors in quadrature we get total uncertainties of about $\pm 10\%$ for all three values of δ. For the total branching ratio in the Standard Model we obtain $\text{B}(B \to X_s\gamma) = (3.29 \pm 0.33) \times 10^{-4} N_{\text{SL}}$. Contrary to common folklore, about 40% of the branching ratio reflects the presence of the current–current operator O_2 in the effective Hamiltonian and is not related to penguin diagrams with a top-quark loop. For comparison with previous authors, we note that with the choice $\delta = 0.99$ we would obtain $\text{B}(B \to X_s\gamma) = (3.37 \pm 0.34) \times 10^{-4} N_{\text{SL}}$.

3 Implementation of Fermi motion

Whereas the explicit power corrections included in the functions k_{77} and k_{27} in (13) are very small, there is an important nonperturbative effect that has not been included so far in next-to-leading order analyses of the $B \to X_s\gamma$ branching ratio: the residual motion of the b quark inside the B meson caused by its soft interactions with the light constituents leads to a modification of the photon energy spectrum, which is an important effect if a realistic cutoff is imposed [44]. This so-called "Fermi motion" is included in the heavy-quark expansion by resumming an infinite set of leading-twist corrections into a shape function $F(k_+)$, which governs the light-cone momentum distribution of the heavy quark inside the B meson [26–28]. This function shares many similarities with the parton distributions in deeply inelastic scattering. The physical decay distributions are obtained from a convolution of parton model spectra with this function. In the process, phase-space boundaries defined by parton kinematics are transformed into the proper physical boundaries defined by hadron kinematics. The shape function is a universal, i.e. process-independent characteristic of the B meson governing the inclusive decay spectra in processes with massless partons in the final state, such as $B \to X_s\gamma$ and $B \to X_u\,\ell\,\nu$. It is important to note that this function does not describe in an accurate way the distributions in decays into massive partons such as $B \to X_c\,\ell\,\nu$ [27,28]. Unfortunately, therefore, the shape function cannot be determined using the lepton spectrum in semileptonic decays of B mesons, for which high-precision data exist. On the other hand, there is some useful theoretical information on the moments of the shape function, which are related to the forward matrix elements of local operators [26]:

$$A_n = \int \mathrm{d}k_+\, k_+^n\, F(k_+) = \frac{1}{2m_B}\,\langle B|\,\bar b\,(iD_+)^n b\,|B\rangle\,. \quad (21)$$

The first three moments satisfy $A_0 = 1$, $A_1 = 0$ and $A_2 = \frac{1}{3}\mu_\pi^2$, where $\mu_\pi^2 = -\lambda_1$ is related to the kinetic energy of the b quark inside the B meson [39]. The condition $A_1 = 0$, which is a consequence of the equations of motion, ensures that the quark mass m_b entering our theoretical expressions is the pole mass (defined to the appropriate order in perturbation theory, i.e. to one-loop order for our purposes).

Let $P_{\text{p}}(y_{\text{p}})$ be the photon energy spectrum in the parton model, where $y_{\text{p}} = 2E_\gamma/m_b$ with $0 \le y_{\text{p}} \le 1$. Our goal is to include the effects of Fermi motion and calculate the physical spectrum $P(y)$ as a function of the variable $y = 2E_\gamma/m_B$. To leading-twist approximation, the result is given by the convolution [26]

$$P(y)\,\mathrm{d}y = \int \mathrm{d}k_+\, F(k_+)\,\Big[P_{\text{p}}(y_{\text{p}})\,\mathrm{d}y_{\text{p}}\Big]_{y_{\text{p}}=y_{\text{p}}(k_+)}\,, \quad (22)$$

where $y_{\text{p}}(k_+)$ is obtained by replacing m_b in the definition of y_{p} with the "effective mass" $m_b^* = m_b + k_+$ [28], i.e. $y_{\text{p}}(k_+) = 2E_\gamma/m_b^* = y m_B/m_b^*$. Because the support of the shape function is restricted to the range $-m_b \le k_+ \le m_B - m_b$, it follows that $0 \le y \le 1$. In other words, after the inclusion of Fermi motion the spectrum extends to the true kinematic endpoint at $E_\gamma^{\max} = m_B/2$. Let us denote by $B_{\text{p}}(\delta_{\text{p}})$ the integrated branching ratio calculated in the parton model, which is given by an integral over the spectrum $P_{\text{p}}(y_{\text{p}})$ with a cutoff δ_{p} defined by the condition that $E_\gamma \ge \frac{1}{2}(1-\delta_{\text{p}})m_b$. From (22), it then follows that the corresponding physical quantity $B(\delta)$ with δ defined such that $E_\gamma \ge \frac{1}{2}(1-\delta)m_B$ is given by

$$B(\delta) = \int\limits_{m_B(1-\delta)-m_b}^{m_B-m_b} \mathrm{d}k_+\, F(k_+)\, B_{\text{p}}\!\left(1 - \frac{m_B(1-\delta)}{m_b + k_+}\right). \quad (23)$$

This relation is such that $B(1) = B_{\text{p}}(1)$, implying that the total branching ratio is not affected by Fermi motion; indeed, the $1/m_Q^2$ corrections in (13) are the only power corrections to the total branching ratio. The effects of Fermi motion are, however, important for realistic values of the cutoff. We will now evaluate relation (23) for the various components $B_{ij}(\delta)$ introduced in the previous section.

Several ansätze for the shape function have been suggested in the literature [26–28]. For our purposes, given the poor present knowledge about higher moments A_n with $n \ge 3$, it is sufficient to adopt the simple form

$$F(k_+) = N\,(1-x)^a e^{(1+a)x}\,; \quad x = \frac{k_+}{\bar\Lambda} \le 1\,, \quad (24)$$

Table 3. Values of the coefficients $B_{ij}(\delta)$ in units of 10^{-4}, corrected for Fermi motion

m_b [GeV]	δ	$E_\gamma^{\rm min}$ [GeV]	B_{22}	B_{77}	B_{88}	B_{27}	B_{28}	B_{78}	$\sum B_{ij}$
4.65	0.90	0.26	1.289	0.375	0.014	1.401	0.162	0.083	3.324
	0.30	1.85	1.201	0.333	0.004	1.322	0.132	0.075	3.068
	0.15	2.24	0.802	0.220	0.002	0.889	0.087	0.050	2.050
4.80	0.90	0.26	1.258	0.382	0.014	1.395	0.160	0.083	3.291
	0.30	1.85	1.213	0.352	0.004	1.362	0.134	0.078	3.144
	0.15	2.24	0.945	0.272	0.003	1.071	0.104	0.060	2.456
4.95	0.90	0.26	1.227	0.388	0.014	1.388	0.157	0.083	3.259
	0.30	1.85	1.200	0.365	0.004	1.375	0.133	0.080	3.156
	0.15	2.24	1.072	0.323	0.003	1.239	0.118	0.070	2.825

where $\bar\Lambda = m_B - m_b$. This ansatz is such that $A_1 = 0$ by construction[3], whereas the condition $A_0 = 1$ fixes the normalization N. The parameter a can be related to the second moment, yielding $A_2 = \frac{1}{3}\mu_\pi^2 = \bar\Lambda^2/(1+a)$. Thus, the b-quark mass (or $\bar\Lambda$) and the quantity μ_π^2 (or a) are the two parameters of our function. Below, we will take $m_b = 4.8\,\text{GeV}$ and $\mu_\pi^2 = 0.3\,\text{GeV}^2$ as reference values, in which case $a \approx 1.29$. Because the main effect of Fermi motion is to fill the gap between the parton model endpoint of the photon spectrum and the physical endpoint, it turns out that the results are very sensitive to the choice of the b-quark mass. Table 3 shows the coefficients $B_{ij}(\delta)$ corrected for Fermi motion using the above ansatz with a fixed value $a \approx 1.29$ but different values of m_b. A representative range of parameters is covered by considering the three following cases: $m_b = 4.65\,\text{GeV}$ (yielding $\bar\Lambda \approx 0.63\,\text{GeV}$ and $\mu_\pi^2 \approx 0.52\,\text{GeV}^2$), $m_b = 4.8\,\text{GeV}$ (yielding $\bar\Lambda \approx 0.48\,\text{GeV}$ and $\mu_\pi^2 \approx 0.3\,\text{GeV}^2$), and $m_b = 4.95\,\text{GeV}$ (yielding $\bar\Lambda \approx 0.33\,\text{GeV}$ and $\mu_\pi^2 \approx 0.14\,\text{GeV}^2$). We also show the values of the photon energy cutoff, $E_\gamma^{\rm min} = \frac{1}{2}(1-\delta)m_B$, which are now independent of the b-quark mass.

For a graphical illustration of the sensitivity of our results to the parameters of the shape function, we show in the upper plots in Fig. 3 the predictions for the Standard Model branching ratio as a function of the energy cutoff $E_\gamma^{\rm min}$. In the first plot, we use the same sets of parameters as in Table 3, i.e. $m_b = 4.65\,\text{GeV}$ (long-dashed curve), 4.8 GeV (solid curve), and 4.95 GeV (short-dashed curve), with μ_π^2 adjusted such that the ratio $\mu_\pi^2/\bar\Lambda^2$ remains constant. The gray line shows the result obtained using the same parameters as for the solid line, but with a Gaussian ansatz $F(k_+) = N\,(1-x)^c e^{-b(1-x)^2}$ for the shape function. For comparison, we also show the data point $\text{B}(B\to X_s\gamma) = (2.04\pm0.47)\times10^{-4}$ obtained by the CLEO Collaboration with a cutoff at 2.2 GeV [23]. As shown in Appendix B, the fact that in the CLEO analysis the cutoff is imposed on the photon energy in the laboratory frame rather than in the rest frame of the B meson is not very important for the partially integrated branching ratio and has been neglected here. In the second plot, we keep $m_b = 4.8\,\text{GeV}$ fixed and compare the parton model result (gray dotted curve) with the results corrected for Fermi motion, using $\mu_\pi^2 = 0.15\,\text{GeV}^2$ (short-dashed curve), $0.30\,\text{GeV}^2$ (solid curve), and $0.45\,\text{GeV}^2$ (long-dashed curve). This figure illustrates how Fermi motion fills the gap between the parton model endpoint at $m_b/2$ and the physical endpoint at $m_B/2$. To be precise, the physical endpoint is actually located at $[m_B^2 - (m_K + m_\pi)^2]/2m_B \approx 2.60\,\text{GeV}$, i.e. slightly below $m_B/2 \approx 2.64\,\text{GeV}$. Close to the endpoint, our theoretical prediction provides an average description of the true spectrum in the sense of quark–hadron duality (see Sect. 5). Comparing the two upper plots in Fig. 3, we observe that the uncertainty due to the value of the b-quark mass is the dominant one. Variations of the parameter μ_π^2 have a much smaller effect on the partially integrated branching ratio, and also the sensitivity to the functional form adopted for the shape function turns out to be small. This behaviour is a consequence of global quark–hadron duality, which ensures that even partially integrated quantities are rather insensitive to bound-state effects. The strong remaining dependence on the b-quark mass is simply due to the transformation by Fermi motion of phase-space boundaries from parton to hadron kinematics. We believe that the spread of results obtained by varying m_b between 4.65 and 4.95 GeV (with μ_π^2 adjusted as described above) is a fair representation of the amount of model dependence resulting from the inclusion of Fermi motion. With a cutoff $E_\gamma^{\rm min} = 2.2\,\text{GeV}$ as used in the CLEO analysis, and correcting for the small effect of the boost from the B rest frame to the laboratory frame (see Appendix B), we obtain

$$\text{B}(B\to X_s\gamma)\big|_{E_\gamma^{\rm lab}>2.2\,\text{GeV}} = (2.57\pm0.26^{+0.31}_{-0.36})\times10^{-4} N_{\rm SL}\,. \tag{25}$$

The first error accounts for the dependence on the various input parameters, while the second one reflects the uncertainty due to the modeling of Fermi motion. For a cutoff as high as that employed in the CLEO analysis, this uncertainty is in fact the dominant theoretical error. In the future, an effort should therefore be made to lower the cutoff on the photon energy to a value of 2 GeV or less. Comparing our result with the CLEO measurement of $(2.04\pm0.47)\times10^{-4}$ [23], we obtain the ratio $R = \text{B}_{\rm exp}/\text{B}_{\rm th} = 0.79\pm0.18(\text{exp})^{+0.14}_{-0.12}(\text{th})$ (assuming $N_{\rm SL} = 1$),

[3] For simplicity, we neglect exponentially small terms in $m_b/\bar\Lambda$

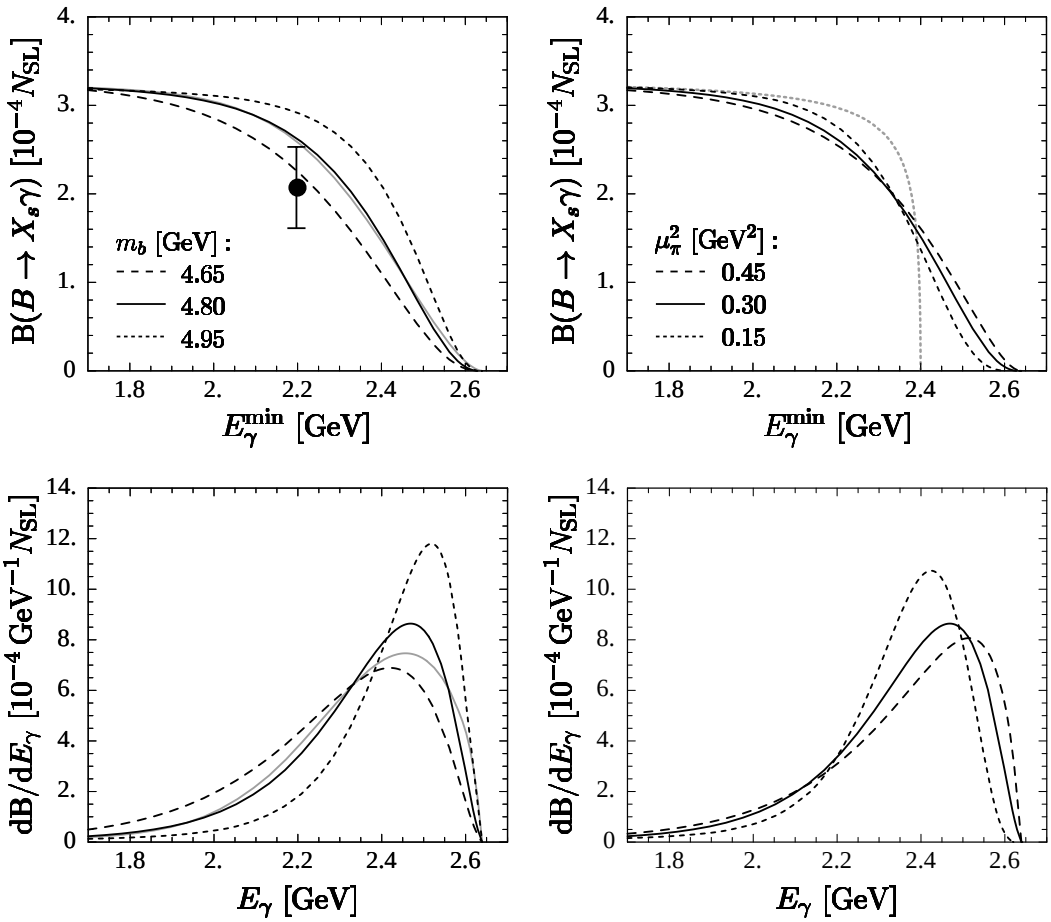

Fig. 3. Theoretical predictions for the integrated $B \to X_s\gamma$ branching ratio (upper plots) and the corresponding photon spectra (lower plots) for various choices of the shape-function parameters $(m_b,\, \mu_\pi^2)$ and functional form, as explained in the text. The calculation of the photon spectra will be discussed in Sect. 4

which deviates from unity by less than one standard deviation. This must be confronted with the comparison of the total branching ratios using the value reported in (1), which gives $R = \mathrm{B}_{\mathrm{exp}}/\mathrm{B}_{\mathrm{th}} = 0.71 \pm 0.20(\mathrm{exp}) \pm 0.07(\mathrm{th})$. The extrapolation to low photon energies performed in the CLEO analysis [1] has artificially increased the deviation from the theoretical prediction by a significant amount, i.e. the model dependence inherent in this extrapolation has been underestimated. This is also reflected in the fact that the correction factor relating the total branching ratio to the branching ratio obtained with the cut $E_\gamma^{\mathrm{lab}} > 2.2\,\mathrm{GeV}$ is $K_{2.2} = 0.78^{+0.09}_{-0.11}$, which differs significantly from the factor 0.87 ± 0.06 employed by CLEO. Using our correction factor, the extrapolation of the CLEO measurement to the total branching ratio yields

$$\mathrm{B}(B \to X_s\gamma)_{\mathrm{CLEO}} = (2.62 \pm 0.60_{\mathrm{exp}}\,{}^{+0.37}_{-0.30\,\mathrm{th}}) \times 10^{-4} \tag{26}$$

instead of the value quoted in (1). We stress that the change in the central value and the increase of the theoretical error[4] with respect to the result reported by CLEO are entirely due to the improved treatment of bound-state effects presented in this paper. Whereas the CLEO analysis relies on a quark model, we perform an analysis that is entirely based on QCD and the operator product expansion. Our treatment is thus not only more conservative but also more consistent from a theoretical point of view.

The procedure of extrapolating a measurement of the $B \to X_s\gamma$ branching ratio in the region of high photon energies to the total branching ratio not only introduces large systematic errors, but also entails the disadvantage that one has to rely on the Standard Model to describe the photon spectrum in the low-energy region. In our opinion, it would therefore be desirable if in the future the comparison of theory with experiment were done for the partially integrated branching ratio, which is the quantity actually measured, rather than for the total branching ratio.

[4] The second error quoted in (1) is dominated by experimental systematics. The theoretical error was assumed to be $\pm 0.16 \times 10^{-4}$

4 Photon spectrum and determination of m_b

The large theoretical uncertainties in the calculation of Fermi motion effects on the partially integrated branching ratio for $B \to X_s\gamma$ decays can be reduced in two ways. The first possibility is to lower the cutoff $E_\gamma^{\rm min}$ on the photon energy. As is apparent from Fig. 3, if a value as low as $E_\gamma^{\rm min} \lesssim 2\,\text{GeV}$ could be achieved, the theoretical prediction would become insensitive to the parameters of the shape function. To what extent this will be possible in future experiments depends on their capability to reject the background of photons from other decays. The Cabibbo-favoured B decays into charmed particles, in particular, can yield photons of energy up to about 2.3 GeV. The second possibility is that future high-precision measurements of the photon spectrum will make it possible to adjust the parameters of the shape function from a fit to the data. We repeat that these parameters cannot be determined from a study of the lepton spectrum in $B \to X_c\,\ell\,\nu$ decays. On the other hand, a determination of the shape-function parameters from $B \to X_s\gamma$ decays would enable us to predict the lepton spectrum in $B \to X_u\,\ell\,\nu$ in a model-independent way [26]. This may help to reduce the theoretical uncertainty in the current value of $|V_{ub}|$. A detailed analysis of the photon spectrum will therefore be an important aspect in future analyses of inclusive radiative B decays.

Given the expression for the integrated $B \to X_s\gamma$ branching ratio derived in the previous sections, the photon spectrum can be obtained from differentiation with respect to δ, i.e.

$$\begin{aligned} P(y) &= \frac{1}{\text{B}(B \to X_c\,e\,\bar\nu)}\,\frac{\text{dB}(B \to X_s\gamma)}{\text{d}y} \\ &= \frac{6\alpha}{\pi f(z)}\,\left|\frac{V_{ts}^* V_{tb}}{V_{cb}}\right|^2\,K'_{\rm NLO}(1-y)\,, \end{aligned} \tag{27}$$

where $y = E_\gamma/E_\gamma^{\rm max}$. In analogy with (7), we write

$$\begin{aligned} K'_{\rm NLO}(1-y) = &\sum_{\substack{i,j=2,7,8\\ i\le j}} p_{ij}(y,\mu_b)\,\text{Re}\Big[C_i^{(0)}(\mu_b)\,C_j^{(0)*}(\mu_b)\Big] \\ &+\Delta(y)\,\frac{\alpha_s(\mu_b)}{2\pi}\,\text{Re}\Big[C_7^{(1)}(\mu_b)\,C_7^{(0)*}(\mu_b)\Big] \\ &+\Delta(y)\frac{\alpha}{\alpha_s(\mu_b)}\Big(2\,\text{Re}\Big[C_7^{(\rm em)}(\mu_b)\,C_7^{(0)*}(\mu_b)\Big] \\ &-k_{\rm SL}^{(\rm em)}(\mu_b)\,|C_7^{(0)}(\mu_b)|^2\Big)\,, \end{aligned} \tag{28}$$

where

$$\begin{aligned} \Delta(y) = &-\frac{4\alpha_s(\mu_b)}{3\pi(1-y)}\left(\ln(1-y)+\frac{7}{4}\right) \\ &\times\exp\left[-\frac{2\alpha_s(\mu_b)}{3\pi}\left(\ln^2(1-y)+\frac{7}{2}\ln(1-y)\right)\right] \end{aligned} \tag{29}$$

is the derivative of the Sudakov factor. The Sudakov factor can be regarded as a smeared step function, and hence $\Delta(y)$ can be viewed as a smeared δ-function. Hence, we must consider $\Delta(y) = O(1)$ rather than $O(\alpha_s)$, in spite of the prefactor α_s in (30). The coefficient functions $p_{ij}(y,\mu_b)$ in (28) have the same form as the coefficients $k_{ij}(\delta,\mu_b)$ in (13) but with the replacements $S(\delta) \to \Delta(y)$ and $f_{ij}(\delta) \to s_{ij}(y)$, where $s_{ij}(y) = f'_{ij}(1-y)$. The explicit expressions for these functions are presented in Appendix C.

Given the photon spectrum $P_{\rm p}(y_{\rm p})$ in the parton model, where $y_{\rm p} = 2E_\gamma/m_b$, the next step is to implement Fermi motion. According to (22), this is achieved by taking the convolution

$$P(y) = \int\limits_{m_B y - m_b}^{m_B - m_b} \text{d}k_+\,F(k_+)\,\frac{m_B}{m_b+k_+}\,P_{\rm p}\left(\frac{m_B y}{m_b+k_+}\right)\,, \tag{30}$$

where $y = 2E_\gamma/m_B$. It is convenient to decompose the final result for the spectrum in a form analogous to (20) by writing

$$\begin{aligned} &\frac{1}{N_{\rm SL}}\,\frac{\text{dB}(B \to X_s\gamma)}{\text{d}E_\gamma} \\ &\quad= 0.105 \times \frac{2}{m_B}\,P(2E_\gamma/m_B) \\ &\quad= P_{22}(E_\gamma) + P_{77}(E_\gamma)\left(|\xi_7|^2 + |\xi_7^R|^2\right) \\ &\qquad+P_{88}(E_\gamma)\left(|\xi_8|^2 + |\xi_8^R|^2\right) \\ &\qquad+P_{27}(E_\gamma)\,\text{Re}(\xi_7) + P_{28}(E_\gamma)\,\text{Re}(\xi_8) \\ &\qquad+P_{78}(E_\gamma)\left[\text{Re}(\xi_7\xi_8^*) + \text{Re}(\xi_7^R\xi_8^{R*})\right]\,. \end{aligned} \tag{31}$$

The results for the various components of the spectrum are shown in Fig. 4, where we take central values of all input parameters. The contributions are ordered according to their magnitude. In the last plot, we show all components together on a logarithmic scale. Note that, with the exception of the tiny 8-8 contribution, the different components have a very similar spectral shape. This observation implies that the shape of the photon spectrum is not sensitive to physics beyond the Standard Model. With a realistic cutoff on the photon energy, even large deviations of the parameters $\xi_7^{(R)}$ and $\xi_8^{(R)}$ from their standard values would not have a detectable effect on the shape of the photon spectrum. Although this may be disappointing from the point of view of searching for New Physics in $B \to X_s\gamma$ decays, it entails the advantage that a precise measurement of the spectrum can be used to determine the parameters of the shape function without relying on the Standard Model. For the remainder of this section we concentrate on the Standard Model, for which the photon spectrum is given by the sum of the individual contributions shown in Fig. 4. The results obtained for various choices of the parameters of the shape function are shown in the lower plots in Fig. 3. The photon spectra are more sensitive to the functional form of the shape function than are the predictions for the integrated branching ratio in the upper plots. Therefore, a fit to future high-precision data on the spectrum should use a more flexible ansatz for the shape function than the one given in (24). On the

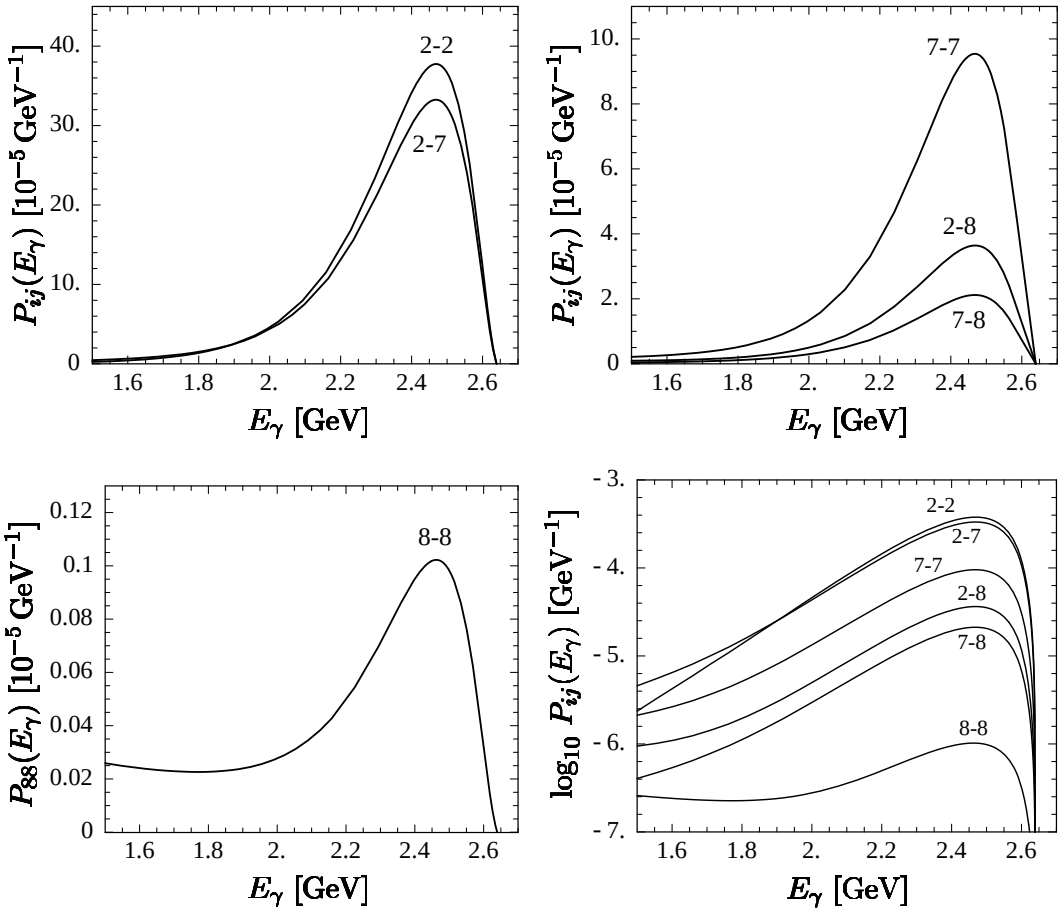

Fig. 4. Different components of the photon spectrum in $B \to X_s\gamma$ decays

other hand, we will see below that even a small element of smearing provided, e.g., by the finite detector resolution or the Lorentz boost of photons from the B rest frame to the laboratory frame, is sufficient to reduce this sensitivity significantly.

Let us now make a comparison of our predictions for the photon energy spectrum with the data obtained by the CLEO Collaboration, which are presented in Table 4. To this end, we must take into account that B mesons produced in decays of the $\Upsilon(4s)$ resonance have a small momentum in the laboratory system, so that the photon spectrum is Doppler shifted. The boost that connects the B rest frame with the laboratory frame is characterized by

$$\beta = \frac{|\mathbf{p}_B|}{E_B} = \sqrt{1 - \frac{4m_B^2}{m_{\Upsilon(4s)}^2}} = 0.064 \pm 0.007\,, \qquad (32)$$

and the maximum energy in the laboratory frame is $(E_\gamma^{\rm lab})_{\rm max} \approx (1+\beta)E_\gamma^{\rm max} \approx E_\gamma^{\rm max} + 170\,{\rm MeV}$. The formalism for incorporating this effect is discussed in Appendix B. The results are shown in the left-hand plot in Fig. 5, where we compare the corrected photon spectra with the CLEO data, using our standard parameters for the shape function. No fit to the data has been performed;

Table 4. CLEO results for the photon spectrum in $B \to X_s\gamma$ decays [23]. The value of the branching ratio reported in [1] was obtained from the middle two bins

$\Delta E_\gamma^{\rm lab}$ [GeV]	${\rm d}B/{\rm d}E_\gamma^{\rm lab}$ [$10^{-4}\,{\rm GeV}^{-1}$]
1.95–2.20	2.13 ± 2.38
2.20–2.45	4.50 ± 1.52
2.45–2.70	3.54 ± 0.98
2.70–2.95	0.11 ± 0.54

in all cases, the theoretical spectra are normalized to the central Standard Model value of 3.29×10^{-4} for the total branching ratio (assuming $N_{\rm SL} = 1$). Note that after the smearing implied by the Doppler shift of the spectra, the gray and the black solid lines, which as before correspond to different functional forms adopted for the shape function, are very close together. This reflects the reduced sensitivity to the fine details of the modeling of Fermi motion, which is achieved by any kind of smearing of the photon spectrum.

To perform a fit to the data, we rebin our theoretical results in the same energy intervals as used by CLEO and, for each set of parameters for the shape function, adjust

Table 5. Results for the total $B \to X_s\gamma$ branching ratio, and upper limits at 90% confidence level, obtained from a fit to the CLEO data shown in Table 4. The quantity R denotes the ratio of the extracted value for the branching ratio to the Standard Model prediction

	$m_b = 4.65\,\text{GeV}$	$m_b = 4.80\,\text{GeV}$	$m_b = 4.95\,\text{GeV}$
$\text{B}(B \to X_s\gamma)$ $[10^{-4}]$	3.09 ± 0.66	2.66 ± 0.56	2.18 ± 0.47
90% CL	< 4.66	< 4.06	< 3.26
$\chi^2/n_{\rm dof}$	0.64/3	0.08/3	0.97/3
R	$0.94 \pm 0.20 \pm 0.09$	$0.81 \pm 0.17 \pm 0.08$	$0.66 \pm 0.14 \pm 0.07$

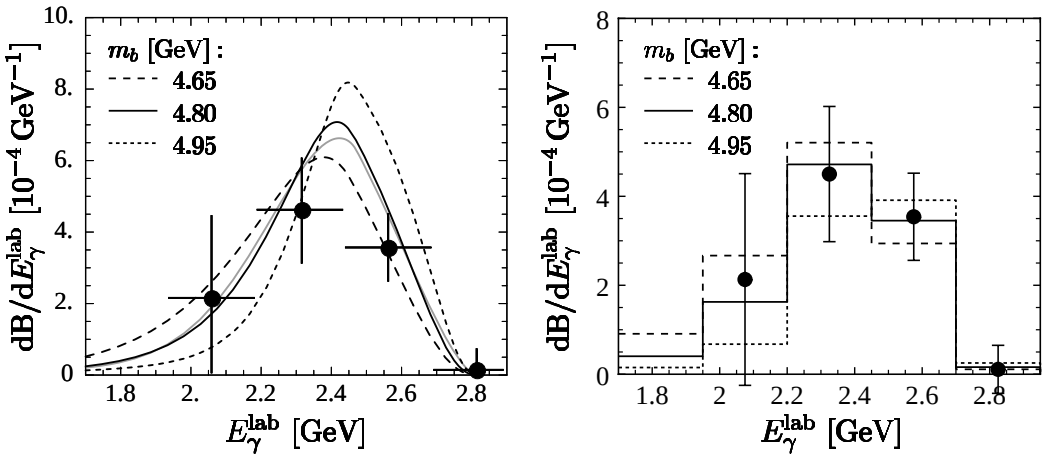

Fig. 5. Theoretical predictions for the photon energy spectrum in the laboratory frame for different parameters of the shape function. The gray line in the left-hand plot shows the result obtained using a Gaussian form of the shape function with central values of m_b and μ_π^2. The data points show the CLEO results. In the left-hand plot, no fit to the data is performed, whereas the right-hand plot shows the results of the best fits reported in Table 5

the overall normalization (i.e. the total branching ratio) to give the best fit to the data. The results are reported in Table 5, and the best fits displayed in the right-hand plot in Fig. 5. All fits have an excellent $\chi^2/n_{\rm dof} \ll 1$, indicating that with the present accuracy of the data it is not possible to determine the parameters of the shape function in a meaningful way. Unless a very large value of m_b is chosen, the result for the total branching ratio comes out higher than the value (1) reported by CLEO, and the upper bounds for the branching ratio obtained at 90% confidence level are well above the Standard Model prediction of $(3.29 \pm 0.33) \times 10^{-4}$. Combining the results obtained for the three choices of m_b, we get

$$\text{B}(B \to X_s\gamma)^{\rm spectrum}_{\rm CLEO} = (2.66 \pm 0.56_{\rm exp}\,{}^{+0.43}_{-0.48\,\rm th}) \times 10^{-4}\,, \tag{33}$$

corresponding to a ratio $R = \text{B}_{\rm exp}/\text{B}_{\rm th} = 0.81 \pm 0.17\,(\text{exp})^{+0.13}_{-0.15}(\text{th})$, which deviates from unity by less than one standard deviation. In quoting the theoretical error we assume that the spread of the results shown in the three columns of Table 5 represents a reasonable estimate of the theoretical uncertainty arising from the modeling of the shape function. The individual R ratios for the different choices of m_b are displayed in the last column in the table. The result (33) is in good agreement with the value (26) obtained from the extrapolation of the partially integrated branching ratio measured by CLEO with a photon energy cutoff at 2.2 GeV. Since the fit to the photon spectrum uses more experimental information, we tend to consider (33) to be the more conservative result of the two. We will therefore use this value in our further analysis.

Once high-statistic measurements of the photon spectrum become available, it will be possible to determine the parameters of the shape function directly from the data. In particular, the average photon energy in $B \to X_s\gamma$ decays is a sensitive measure of the b-quark mass. In practice, what can be measured is the average photon energy as a function of the cutoff $E_\gamma^{\rm min}$, given by

$$\langle E_\gamma \rangle = \frac{\int\limits_{E_\gamma^{\rm min}}^{E_\gamma^{\rm max}} \mathrm{d}E_\gamma\, E_\gamma\, \dfrac{\mathrm{dB}}{\mathrm{d}E_\gamma}}{\int\limits_{E_\gamma^{\rm min}}^{E_\gamma^{\rm max}} \mathrm{d}E_\gamma\, \dfrac{\mathrm{dB}}{\mathrm{d}E_\gamma}}\,. \tag{34}$$

Provided that $E_\gamma^{\rm min}$ is not too close to the endpoint, this quantity is insensitive to the details of the shape function except for the value of m_b. Indeed, at leading order in the heavy-quark expansion one simply gets $\langle E_\gamma \rangle = m_b/2$. The

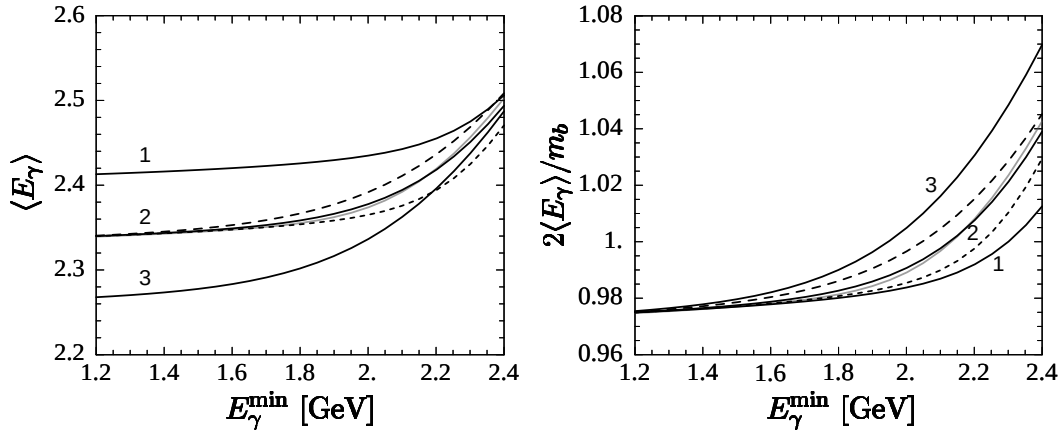

Fig. 6. Theoretical predictions for the average photon energy as a function of the cutoff $E_\gamma^{\rm min}$, for different parameters of the shape function. The solid lines refer to: (1) $m_b = 4.95\,\text{GeV}$ and $\mu_\pi^2 = 0.14\,\text{GeV}^2$; (2) $m_b = 4.8\,\text{GeV}$ and $\mu_\pi^2 = 0.3\,\text{GeV}^2$; (3) $m_b = 4.65\,\text{GeV}$ and $\mu_\pi^2 = 0.52\,\text{GeV}^2$. The dashed lines show the dependence on the value of μ_π^2 for the case $m_b = 4.8\,\text{GeV}$, where $\mu_\pi^2 = 0.3\,\text{GeV}^2$ (*solid*), $0.45\,\text{GeV}^2$ (*long-dashed*), $0.15\,\text{GeV}^2$ (*short-dashed*). The gray lines refer to the Gaussian ansatz for the shape function

result for the average photon energy obtained by including the full next-to-leading order corrections is shown in Fig. 6. For simplicity, we neglect in this figure the boost between the B rest frame and the laboratory frame, which has a very small effect on the average photon energy. The different curves in each plot refer to the various sets of shape-function parameters considered previously in Fig. 3. In the right-hand plot we show the average photon energy normalized to $m_b/2$. We observe that for $E_\gamma^{\rm min} \lesssim 1.8\,\text{GeV}$ the mean photon energy provides a sensitive measure of the mass of the b quark, which to a good approximation is independent of other shape-function parameters such as μ_π^2. Asymptotically, for very small cutoff values $\langle E_\gamma\rangle$ is lower than $m_b/2$ by about 3%. For $E_\gamma^{\rm min} \gtrsim 1.8\,\text{GeV}$, on the other hand, the sensitivity to the modeling of Fermi motion quickly increases. For a cutoff at 2.2 GeV as employed in the CLEO analysis, there is very little sensitivity to the value of m_b.

Moments of the type shown in (34) have been considered previously by Kapustin and Ligeti [45] employing the heavy-quark expansion but not including the effects of Fermi motion. These authors make predictions for the average photon energy and for the width of the photon spectrum for cutoff values between 1.8 and 2.2 GeV. Our findings show that for $E_\gamma^{\rm min} > 1.8\,\text{GeV}$ there are significant corrections to these predictions caused by Fermi motion. This has also been noted by Bauer [46].

Let us assume that in the future it will be possible to measure the average photon energy in $B \to X_s\gamma$ decays with a cutoff low enough to be insensitive to Fermi motion effects. It is instructive to understand the precise meaning of the b-quark mass that can then be extract from the data. In the limit where Fermi motion can be neglected, it follows from (30) that

$$\langle E_\gamma\rangle = \frac{m_b}{2} \times \frac{\int\limits_{1-\delta_{\rm p}}^{1} {\rm d}y_{\rm p}\, y_{\rm p}\, P_{\rm p}(y_{\rm p})}{\int\limits_{1-\delta_{\rm p}}^{1} {\rm d}y_{\rm p}\, P_{\rm p}(y_{\rm p})}\,, \tag{35}$$

where m_b is the pole mass, $P_{\rm p}(y_{\rm p})$ is the photon spectrum in the parton model, and $1-\delta_{\rm p} = 2E_\gamma^{\rm min}/m_b$. Using that

$$\int\limits_{1-\delta_{\rm p}}^{1} {\rm d}y_{\rm p}\, y_{\rm p}\, P_{\rm p}(y_{\rm p}) = \int\limits_0^{\delta_{\rm p}} {\rm d}z \int\limits_{1-z}^{1} {\rm d}y_{\rm p}\, P_{\rm p}(y_{\rm p}) + (1-\delta_{\rm p}) \int\limits_{1-\delta_{\rm p}}^{1} {\rm d}y_{\rm p}\, P_{\rm p}(y_{\rm p})\,, \tag{36}$$

we find for the average photon energy

$$\langle E_\gamma\rangle = \frac{m_b}{2}\, C_E[\alpha_s(m_b)] \times \left\{1 + \frac{\alpha_s(m_b)}{\pi}\, D(\delta_{\rm p}) + \delta_{\rm HT} + \ldots\right\}, \tag{37}$$

where

$$C_E[\alpha_s] = 1 - \frac{23}{54}\,\frac{\alpha_s}{\pi} + O(\alpha_s^2) \approx 0.97\,,$$
$$D(\delta_{\rm p}) = \bar d_{77}(\delta_{\rm p}) + \sum_{\substack{i,j=2,7,8\\ i\le j}}{}' d_{ij}(\delta_{\rm p}) \times \frac{{\rm Re}[C_i^{(0)}(m_b) C_j^{(0)*}(m_b)]}{|C_7^{(0)}(m_b)|^2}\,. \tag{38}$$

The prime on the sum indicates that $(i,j) \neq (7,7)$. The functions $d_{ij}(\delta_{\rm p})$ and $\bar d_{77}(\delta_{\rm p})$ are collected in Appendix C.

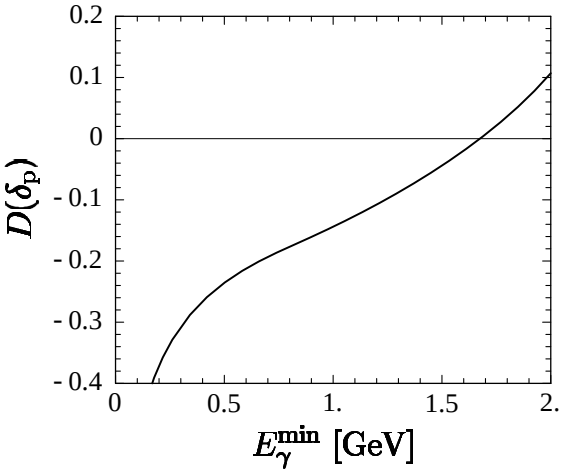

Fig. 7. Theoretical prediction for the function $D(\delta_{\rm p})$

The normalization of $\bar{d}_{77}$ is such that $\bar{d}_{77}(1) = 0$, i.e. apart from corrections due to operator mixing the average photon energy without any cutoff is given by $\frac{1}{2} m_b C_E[\alpha_s]$. Finally, the quantity $\delta_{\rm HT}$ in (37) parametrizes "higher-twist corrections", which are neglected in our leading-twist approximation to the shape function. An explicit calculation of these corrections gives [6,26]

$$\delta_{\rm HT} = -\frac{\lambda_1 + 3\lambda_2}{2m_b^2} \approx (-0.1 \pm 0.4)\% \,, \tag{39}$$

where we have assumed that $-\lambda_1 = \mu_\pi^2 = (0.3 \pm 0.2)\,{\rm GeV}^2$. The contribution of $\delta_{\rm HT}$ in (37) has a negligible effect.

In Fig. 7, the function $D(\delta_{\rm p})$ with $\delta_{\rm p} = 1 - 2E_\gamma^{\rm min}/m_b$ is shown over a wide range of cutoff values. For all realistic values of $E_\gamma^{\rm min}$ this function takes very small values. The corresponding contribution to $\langle E_\gamma \rangle$ in (37) is typically less than 1% and thus negligible. Therefore, to an excellent approximation the average photon energy in $B \to X_s\gamma$ decays measures the product of the b-quark pole mass times the perturbative series $C_E[\alpha_s(m_b)]$, which we have computed to $O(\alpha_s)$:

$$\langle E_\gamma \rangle \approx \frac{m_b}{2}\, C_E[\alpha_s(m_b)] \equiv \frac{1}{2}\, m_b^{(E)} \,. \tag{40}$$

It is well-known that the pole mass of a heavy quark is an infrared-sensitive quantity, which cannot be unambiguously defined beyond perturbation theory [47,48]. Formally, this property appears as a factorial divergence of the expansion coefficients (i.e. an infrared renormalon) in any perturbative series that relates the pole mass to a short-distance mass, such as the running mass $\overline{m}_b(m_b)$ in the $\overline{MS}$ subtraction scheme. On the other hand, the average photon energy in radiative B-meson decays is a physical observable and as such does not suffer from any ambiguity. Therefore, the quantity $m_b^{(E)}$ defined in (40) has a short-distance nature. Indeed, it can be shown that the renormalon in the pole mass is exactly cancelled by a renormalon (i.e. a factorial divergence) in the perturbative series $C_E[\alpha_s]$ [42]. In other words, the short-distance mass $m_b^{(E)}$ can be related to any other short-distance mass without encountering large perturbative coefficients. In particular, we note that

$$m_b^{(E)} = \overline{m}_b(m_b) \left(1 + \frac{49}{54}\, \frac{\alpha_s(m_b)}{\pi} + \dots \right) . \tag{41}$$

Thus, in principle an accurate measurement of the photon spectrum in $B \to X_s\gamma$ decays would provide for a theoretically clean determination of the b-quark mass. In practice, this determination will probably be limited by experiment and may not be competitive with precision determinations of m_b from the analysis of the Υ spectrum.

5 Hadronic mass distribution

In $B \to X_s\gamma$ decays, the invariant mass of the hadronic final state is related with the photon energy in the B rest frame through $M_H^2 = m_B^2 - 2m_B E_\gamma$. Therefore, our theoretical results for the photon spectrum can be translated into predictions for the hadronic mass spectrum. Since experimentally the measurements of the photon energy and hadronic mass spectra are quite different, it may be useful to discuss our results also in terms of the variable M_H. In the left-hand plot in Fig. 8, we show the corresponding spectra obtained using our standard choices for the parameters of the shape function.

At this point, it may be worthwhile to recall that the theoretical predictions for the photon energy and hadronic mass spectra must be understood in the sense of quark–hadron duality. In particular, the true hadronic mass spectrum in the low-mass region may have resonance structures due to low-lying kaon states, and thus may look rather different from our theoretical predictions. To discuss in more detail how quark–hadron duality works in the present case we distinguish two kinematic regions: the "endpoint region" and the "resonance region". The endpoint region of the photon energy spectrum is characterized by the condition that $E_\gamma^{\rm max} - E_\gamma = O(\bar{\Lambda})$, where $\bar{\Lambda} = m_B - m_b$. It is in this region that the effects of Fermi motion are relevant and determine the shape of the spectrum. In the endpoint region, the invariant mass of the hadronic final state is of order $m_B \bar{\Lambda} \gg \Lambda_{\rm QCD}^2$, implying that a large number of final states are kinematically accessible. Under such circumstances, local quark–hadron duality ensures that the photon and hadronic mass spectra are similar to the corresponding inclusive spectra predicted by the heavy-quark expansion even without applying a smearing procedure. In the resonance region, on the other hand, the invariant mass of the hadronic final state is of order $\Lambda_{\rm QCD}^2$, implying that the photon energy is very close to the kinematic endpoint: $E_\gamma^{\rm max} - E_\gamma = O(\Lambda_{\rm QCD}^2/m_B)$. The heavy-quark expansion does not allow us to make model-independent predictions for the structure of the individual resonance contributions. Global quark–hadron duality can, however, be restored by averaging the spectra over a

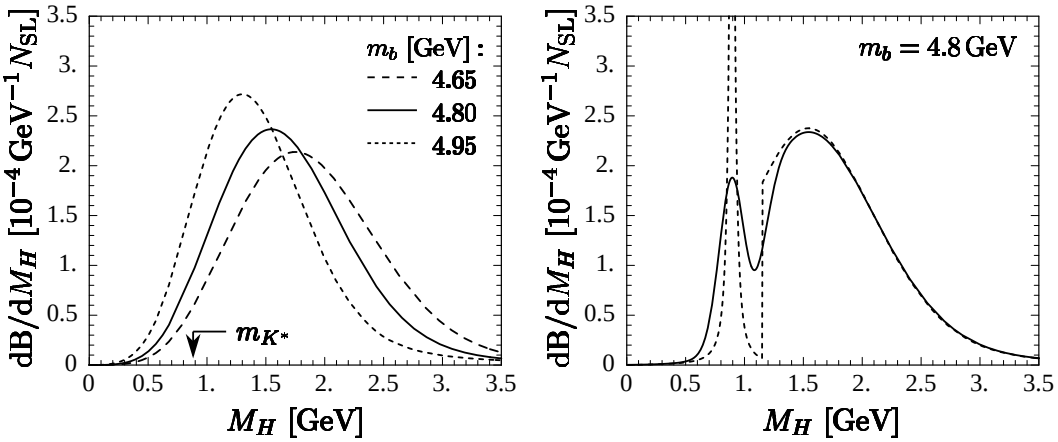

Fig. 8. Theoretical predictions for the invariant hadronic mass spectrum for different parameters of the shape function

Table 6. Mean masses and widths of the lowest-lying hadronic states accessible in $B \to X_s\gamma$ decays [50], and the corresponding photon energies (errors refer to changing M_H by $\pm\Gamma_H$)

State H	M_H [GeV]	Γ_H [MeV]	E_γ [GeV]
$K\,(n\pi)$	≥ 0.629	continuum	≤ 2.60
$K^*(892)$	0.894	50	2.56 ± 0.01
$K_1(1270)$	1.273	90	2.49 ± 0.02
$K_1(1400)$	1.402	174	2.45 ± 0.05
$K^*(1410)$	1.412	227	2.45 ± 0.06
$K_2^*(1430)$	1.428	103	2.45 ± 0.03
$K_2(1580)$	1.580	110	2.40 ± 0.03
$K_1(1650)$	1.650	150	2.38 ± 0.05
$K^*(1680)$	1.714	323	2.36 ± 0.10
$K_2(1770)$	1.773	186	2.34 ± 0.06

sufficiently wide energy interval, whose size is determined by the average level spacing between the resonance states [49]. We will see below that in the present case the smearing should be done over an interval $\Delta M_H^2 \approx 2\,\text{GeV}^2$, corresponding to an energy interval $\Delta E_\gamma \approx 0.2\,\text{GeV}$. Note that in the case of the CLEO data such an averaging is automatically provided by the Doppler shift of the spectrum due to the motion of the B mesons produced at the $\Upsilon(4s)$ resonance, and thus the photon spectrum is expected to be dual to the theoretical spectrum over the entire energy range.

To make these statements more precise, consider the properties of the lowest-lying kaon states contributing to $B \to X_s\gamma$ decays, which are collected in Table 6. There are six resonances plus a continuum contribution feeding the photon spectrum in the energy interval between 2.4 and 2.6 GeV. Hence, an average over this interval should be calculable using global quark–hadron duality, although a much finer resolution cannot be obtained. In the hadronic mass spectrum, the $K^*(892)$ peak is clearly separated from the rest; however, the next resonances already have widths exceeding the level spacing and hence are overlapping. Therefore, we expect that local duality allows us to predict the hadronic mass spectrum in the region $M_H \gtrsim 1.5\,\text{GeV}$. Indeed, the pattern of resonances exhibited in Table 6 suggests a simple but realistic model for the hadronic mass spectrum consisting of a single Breit–Wigner peak for the $K^*(892)$ followed by a continuum above a threshold M_{cont}, which is dual to the higher resonance contributions and given by the inclusive spectrum calculated using the heavy-quark expansion. This gives

$$\frac{\text{dB}}{\text{d}M_H} = \frac{2M_H N_{K^*}\,\text{B}(B\to K^*\gamma)}{(M_H^2 - m_{K^*}^2)^2 + m_{K^*}^2\Gamma_{K^*}^2} + \Theta(M_H - M_{\text{cont}})\,\frac{\text{dB}_{\text{incl}}}{\text{d}M_H}\,, \tag{42}$$

where

$$N_{K^*} = \frac{m_{K^*}\Gamma_{K^*}}{\arctan\left(\dfrac{m_{K^*}}{\Gamma_{K^*}}\right) + \dfrac{\pi}{2}} \tag{43}$$

is the normalization of the Breit–Wigner distribution. The exclusive branching ratio for the decay $B \to K^*\gamma$ can either be taken from an independent measurement or determined from a fit to the spectrum itself. The continuum threshold M_{cont} is then fixed by the requirement that the total branching ratio be the same as that predicted by the heavy-quark expansion, yielding the condition

$$\int_0^{M_{\text{cont}}} \text{d}M_H\,\frac{\text{dB}_{\text{incl}}}{\text{d}M_H} = \text{B}(B\to X_s\gamma)\Big|_{E_\gamma > E_{\text{cont}}} \stackrel{!}{=} \text{B}(B\to K^*\gamma)\,, \tag{44}$$

where $E_{\text{cont}} = \frac{1}{2}(m_B^2 - M_{\text{cont}}^2)/m_B$. In order to reduce systematic errors, it will in practice be advantageous to normalize both sides of (44) to the total $B \to X_s\gamma$ branching ratio.

To illustrate this method we consider the central value $m_b = 4.8\,\text{GeV}$ and take from experiment the exclusive branching ratio $\text{B}(B \to K^*\gamma) = (0.45 \pm 0.17) \times 10^{-4}$ [51] normalized to our fit result for the total branching ratio given in (33). This yields $\text{B}(B \to K^*\gamma)/\text{B}(B \to X_s\gamma) = 0.17 \pm 0.08$. The value of the continuum threshold which reproduces the central value of this ratio is $M_{\rm cont} \approx 1.15\,\text{GeV}$, which is close to the position of the second resonance $K_1(1270)$. The dashed line in the right-hand plot in Fig. 8 shows the hadronic mass spectrum obtained from (42) using these parameters. To smoothen out the sharp structures, we take a convolution of this curve with a Gaussian smearing function of width $\sigma_{M_H} = 100\,\text{MeV}$, which resembles the binning and resolution of a realistic experiment. The result is shown by the solid curve, which exhibits a two-peak structure: a narrow peak located at the K^* mass, whose width is determined by the mass resolution of the experiment, is followed by a broad bump containing a large number of overlapping resonances, whose sum is dual to the inclusive spectrum predicted by the heavy-quark expansion. The position of the second peak is determined by the b-quark mass through $M_H^{\rm bump} \approx (m_B \bar\Lambda)^{1/2}$, which is located at 1.6 GeV in the present case. This relation is just a reflection of the fact that the b-quark mass determines the average photon energy in $B \to X_s\gamma$ decays (see Sect. 4). We note that such a two-peak structure is indeed seen in the CLEO data on the hadronic mass distribution [1]; however, in view of the large experimental uncertainties it is premature to perform a detailed comparison with the data.

6 Impact of New Physics and constraints on extensions of the Standard Model

Measurements of the $B \to X_s\gamma$ branching ratio have been used extensively to put constraints on the parameters of various extensions of the Standard Model, such as multi-Higgs models, supersymmetry, or left–right symmetric models (see [30,31] for recent reviews). In many of these extensions, the Wilson coefficients of the dipole operators O_7 and O_8 in the effective weak Hamiltonian receive additional contributions from new flavour physics at a high energy scale. The CLEO measurement of the $B \to X_s\gamma$ branching ratio has been used to extract the magnitudes of the Wilson coefficients $C_7(m_W)$ and $C_8(m_W)$ and to compare the results with various model predictions (see, e.g., [52,53]). Likewise, new dipole operators of non-standard chirality may be induced. In general, such New Physics contributions would enter our analysis through non-standard values of the parameters $\xi_i^{(R)}$ defined in (18) and (19). If these parameters carry non-trivial new weak phases, there is potential for observing a large direct CP asymmetry in the decays $B \to X_s\gamma$, which would be a striking signature for New Physics [44]. Here, we shall discuss the impact of New Physics on the CP-average $B \to X_s\gamma$ branching ratio.

The theoretical predictions for the branching ratio and photon spectrum depend on five real combinations of the parameters $\xi_i^{(R)}$, as shown in (20) and (31). It is convenient to introduce the ratio of New Physics contributions to the chromo-magnetic and magnetic dipole operators as

$$\chi = \frac{\xi_8 - 1}{\xi_7 - 1}\,. \tag{45}$$

A specific New Physics scenario will make a prediction for this quantity. In models with dipole operators of non-standard chirality, we assume that ξ_8^R/ξ_7^R is given by the same ratio χ. Moreover, to simplify the discussion we shall assume that χ is a real parameter. This is a good approximation whenever there is a single dominant New Physics contribution, such as the virtual exchange of a new heavy particle, contributing to both the magnetic and the chromo-magnetic dipole operators [54]. With this assumption, there are only two independent structures appearing in (20) and (31), which can be taken to be $\text{Re}(\xi_7)$ and $|\xi_7|^2 + |\xi_7^R|^2$. Note that the imaginary part of ξ_7 enters only in combination with the right-handed coupling $|\xi_7^R|$, implying that by measuring the total branching ratio alone one will not be able to put constraints on the weak phase of ξ_7.

As we saw in Sect. 4, New Physics contributions are unlikely to alter the spectral shape of the photon spectrum in the experimentally accessible region. We therefore focus our discussion on the total branching ratio and define the ratio

$$R_\gamma = \frac{\text{B}(B \to X_s\gamma)}{\text{B}_{\rm SM}(B \to X_s\gamma)} = \frac{K_{\rm NLO}(\delta)}{K_{\rm NLO}^{\rm SM}(\delta)}\,, \tag{46}$$

which directly measures the deviation from the Standard Model. From our result (33) it follows that at the level of two standard deviations $0.37 < R_\gamma < 1.25$. It will be convenient to define a similar ratio of branching ratios for the rare hadronic decays $B \to X_{sg}$, which are induced by the chromo-magnetic dipole operator, so that

$$R_g = \frac{\text{B}(B \to X_{sg})}{\text{B}_{\rm SM}(B \to X_{sg})} = \frac{|C_8(m_b)|^2 + |C_8^R(m_b)|^2}{|C_8^{\rm SM}(m_b)|^2}\,. \tag{47}$$

Whereas the Standard Model predicts the very small value $\text{B}_{\rm SM}(B \to X_{sg}) \approx 0.2\%$, a much larger branching ratio is attainable in models with enhanced $b \to sg$ transitions [54–56]. This would increase the production of charmless final states in hadronic B decays, which could help to explain the low experimental values of the semileptonic branching ratio and charm yield. Although the systematic errors in the measurements of these quantities are large, the results favour values of $\text{B}(B \to X_{sg})$ of order 10% [57, 58]. On the other hand, the CLEO Collaboration has recently presented a preliminary upper limit on $\text{B}(B \to X_{sg})$ of 6.8% (90% CL) [59]. The limit is increased to 9.0% if more recent charmed baryon and charmonium yields are used [58]. In our graphical analysis below we will present 5% and 10% contours for this branching ratio. Which of these two is considered to be a more realistic upper bound is left to the taste of the reader.

The theoretical predictions for the two ratios R can be written as

$$R_\gamma = 1 + A_1(\chi)\,\Big[\text{Re}(\xi_7) - 1\Big] + A_2(\chi)\,\big(|\xi_7|^2 + |\xi_7^R|^2 - 1\big)\,,$$

Table 7. Approximate ranges of χ values for various New Physics contributions to C_7 and C_8, characterized by the particles in penguin diagrams

New Physics penguins	χ
gluino–squark	2–20
techniscalar	9
charged Higgs–top	1.5–2.4
Higgsino–stop	0.2–2.2
left–right W–top	0.9
scalar diquark–top	$-(0.8$–$1.3)$
neutral scalar–vectorlike quark	-8

$$R_g = 1 + A_3(\chi)\left[\mathrm{Re}(\xi_7) - 1\right] + A_4(\chi)\left(|\xi_7|^2 + |\xi_7^R|^2 - 1\right), \tag{48}$$

where

$$\begin{aligned} A_1(\chi) &= \frac{B_{27} + \chi B_{28} + (1-\chi)B_{78} + 2\chi(1-\chi)B_{88}}{B_{22} + B_{27} + B_{77} + B_{28} + B_{78} + B_{88}} \\ &\approx 0.46 + 0.020\chi - 0.0027\chi^2\,, \\ A_2(\chi) &= \frac{B_{77} + \chi B_{78} + \chi^2 B_{88}}{B_{22} + B_{27} + B_{77} + B_{28} + B_{78} + B_{88}} \\ &\approx 0.11 + 0.025\chi + 0.0013\chi^2\,, \\ A_3(\chi) &= \frac{2\chi(1-\chi+r)}{(1+r)^2} \approx 0.43\chi(1-\chi) + 0.50\chi\,, \\ A_4(\chi) &= \frac{\chi^2}{(1+r)^2} \approx 0.21\chi^2\,, \end{aligned} \tag{49}$$

with $r = \sum_{i=1}^8 \bar{h}_i\,\eta^{a_i - 14/23}/C_8^{(0)}(m_W) \approx 1.16$. The expressions for the functions A_1 and A_2 follow directly from (20), whereas those for A_3 and A_4 follow from the result for $C_8^{(0)}(\mu_b)$ given in (9). Since these functions depend on ratios of coefficient functions, their numerical values are rather stable against variations of the input parameters. The numerical results quoted above are obtained by taking central values of all parameters, and in the case of A_1 and A_2 using $E_\gamma^{\min} = 1.95\,\mathrm{GeV}$ for the cutoff on the photon energy, corresponding to the energy interval covered by the data shown in Table 4 and used to derive the result (33).

Approximate ranges of χ for several illustrative New Physics scenarios with $b \to s\gamma$ and $b \to sg$ penguin diagrams containing new particles in the loop have been discussed in [44][5] and are collected in Table 7. Our aim here is not to carry out a detailed study of each model, but to give the reader an idea of the sizable variation that is possible in χ. In supersymmetric theories, e.g., penguin diagrams with gluino–squark loops imply a positive value of χ, which can be tuned over a large range by adjusting the mass ratio $m_{\tilde{g}}/m_{\tilde{q}}$. A detailed analysis of the $B \to X_s\gamma$ branching ratio in this scenario is presented in [56]. Another example with large positive χ is provided by models with techniscalars of charge $\frac{1}{6}$ [54,60,61], whereas an example with large negative χ is provided by penguin diagrams with new neutral scalars and vectorlike quarks of charge $-\frac{1}{3}$. In general, models with large $|\chi|$ offer the possibility of having a direct CP asymmetry in $B \to X_s\gamma$ decays of as much as 10–50% in a large region of model parameter space [44]. Examples of scenarios which lead to more moderate χ values include left–right symmetric models and multi-Higgs models.

Let us first assume that the New Physics contributions to C_7 and C_8 do not contain new weak phases, and that there are no new operators with non-standard chirality, i.e. $\mathrm{Im}(\xi_7) = \xi_7^R = 0$. In the left-hand plot in Fig. 9, we show as a function of χ the allowed ranges for ξ_7 which satisfy the condition that $0.37 < R_\gamma < 1.25$. We also show as dashed lines the 5% and 10% contours for the $B \to X_{sg}$ branching ratio. There are three different regions to distinguish: (a) for $\chi > 3$ only positive values $\mathrm{Re}(\xi_7) \lesssim 1$ are allowed, which are close to the Standard Model value $\xi_7 = 1$; (b) for $-1 < \chi < 3$ a second branch of large negative values of $\mathrm{Re}(\xi_7)$ is allowed, which have magnitude several times larger than in the Standard Model; (c) for $\chi < -1$ only the first branch remains, and the combined constraints from the $B \to X_s\gamma$ and $B \to X_{sg}$ branching ratios imply that $-1 < \xi_7 < 2.5$. The right-hand plot in Fig. 9 shows the same information in a different way, namely in the plane spanned by the (real) New Physics contributions to the Wilson coefficients $C_7(m_W)$ and $C_8(m_W)$. This figure generalizes the corresponding leading-order results discussed in [52,53,56]. It is evident that for a given New Physics scenario, i.e. for a chosen value of χ, the constraints imposed on the Wilson coefficients are quite non-trivial. An example is provided by the "minimal supergravity model" [62] investigated by Hewett and Wells [53], who perform a scan in the SUSY parameter space finding that $-2.5 < \xi_7 < 5.5$, and $\chi \approx 1$ for choices of parameters yielding sizable New Physics contributions to C_7 and C_8. From Fig. 9 it follows that in this model the constraint from the $B \to X_s\gamma$ branching ratio implies $-0.1 < \xi_7 < 1.2$, which excludes a considerable fraction of the SUSY parameter space, whereas there is no constraint from the experimental bound on the $B \to X_{sg}$ branching ratio. Hence, in the minimal supergravity model the Wilson coefficients must take values close to those predicted by the Standard Model or somewhat smaller.

The situation becomes more complicated if one allows for complex values of the Wilson coefficients arising from new weak phases (i.e. $\mathrm{Im}(\xi_7) \neq 0$), or considers the possibility of having dipole operators with non-standard chirality (i.e. $\xi_7^R \neq 0$) [63]. Three illustrative cases are shown in Fig. 10. Note that for large $|\chi|$ the constraint from the $B \to X_{sg}$ branching ratio is quite non-trivial and puts a stringent upper bound on the combination $[\mathrm{Im}(\xi_7)]^2 + |\xi_7^R|^2$.

7 Conclusions

The inclusive radiative decays $B \to X_s\gamma$ play a key role in testing the Standard Model and probing the structure of possible New Physics. We have presented a detailed

[5] In the notation of this reference $\chi = \xi_{\rm SM}/\xi$ with $\xi_{\rm SM} = -3C_7^{\rm SM}(m_W)/C_8^{\rm SM}(m_W) \approx -6.05$

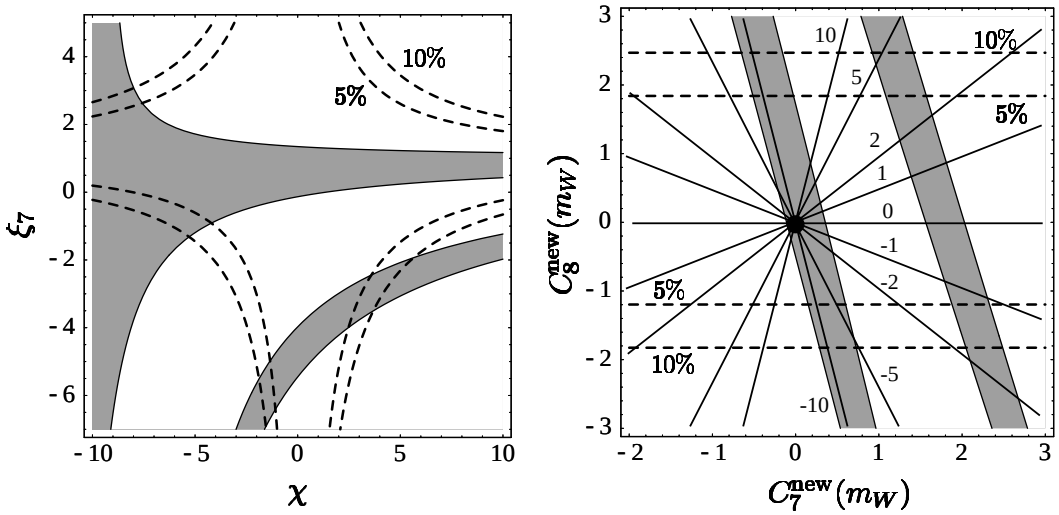

Fig. 9. Regions in parameter space allowed by the experimental constraint on the $B \to X_s\gamma$ branching ratio (*bands*), and contours for the $B \to X_{sg}$ branching ratio (*dashed lines*), assuming $\mathrm{Im}(\xi_7) = \xi_7^R = 0$. The thin lines in the right-hand plot show contours of constant χ values as indicated, the black circle corresponds to the Standard Model result

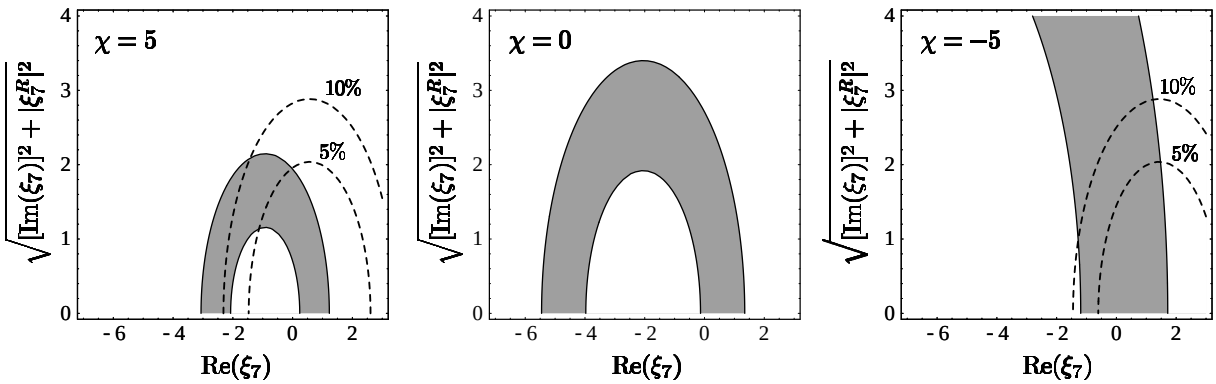

Fig. 10. Regions in parameter space allowed by the experimental constraint on the $B \to X_s\gamma$ branching ratio (*bands*), and contours for the $B \to X_{sg}$ branching ratio (*dashed lines*), in the general case with non-trivial weak phases and/or non-standard chirality operators

study of these decays using the operator product expansion for inclusive decays of heavy hadrons combined with the twist expansion for the description of decay distributions near phase-space boundaries. We have updated (and corrected) the existing next-to-leading order analyses of the total $B \to X_s\gamma$ branching ratio and added several improvements concerning the treatment of QED corrections, the analysis of the renormalization-scale dependence, and the discussion of the sensitivity to New Physics. In particular, we have argued that the truncation error of the perturbative expansion in α_s has been underestimated by previous authors by at least a factor of 2.

Our main focus, however, was to implement a consistent treatment of bound-state effects related to the soft interactions of the b-quark inside the B meson. These effects cause the Fermi motion of the heavy quark, which is responsible for the characteristic shape of the photon energy spectrum in $B \to X_s\gamma$ decays. They lead to the main theoretical uncertainty in the calculation of the inclusive branching ratio if a restriction to the high-energy part of the photon spectrum is imposed. Fermi motion is naturally incorporated in the heavy-quark expansion by resumming an infinite set of leading-twist operators into a non-perturbative shape function. The main theoretical uncertainty in this description lies in the value of the b-quark mass. Other features associated with the detailed functional form of the shape function play only a minor role, particularly if a partial integration over the decay distributions is implied. We have explained how the value of m_b could, in principle, be extracted from a measurement of the average photon energy in $B \to X_s\gamma$ decays. For the Standard Model, we have obtained $\mathrm{B}(B \to X_s\gamma) =$

$(2.57 \pm 0.26^{+0.31}_{-0.36}) \times 10^{-4}$ for the integral over the high-energy part of the photon spectrum with $E_\gamma^{\rm lab} > 2.2\,{\rm GeV}$, where the first error reflects the uncertainty in the input parameters, and the second one the uncertainty in the calculation of Fermi motion. This prediction agrees with the CLEO measurement of the same quantity within one standard deviation. From a reanalysis of the CLEO data, we have obtained values for the total branching ratio that are consistent with the Standard Model prediction of $(3.29 \pm 0.33) \times 10^{-4}$. In the future, an effort should be made to lower the cutoff on the photon energy to a value of 2 GeV or less, even if this would increase the experimental systematic errors. The benefit of such a low cutoff would be that the calculation of the branching ratio becomes insensitive to the effects of Fermi motion, reducing the theoretical uncertainty to the level of 10%.

Besides the photon spectrum, we have studied the invariant hadronic mass distribution in radiative B decays. Investigating the pattern of individual hadron resonances contributing to the spectrum, we have argued that a complementarity between the inclusive theoretical distribution and the true spectrum should set in for $M_H \gtrsim 1.5\,{\rm GeV}$. This leads us to a simple description of the hadronic mass spectrum with only a single parameter, the $B \to K^*\gamma$ branching ratio, to be determined from experiment.

Finally, we have investigated the sensitivity of the $B \to X_s\gamma$ branching ratio and photon spectrum to New Physics beyond the Standard Model and set up a formalism to include possible non-standard contributions in a straightforward way. New Physics contributions enter our predictions through the values of parameters $\xi_i^{(R)}$, which are defined in terms of Wilson coefficient functions at the scale m_W. This formalism allows us to account for non-standard contributions to the magnetic and chromo-magnetic dipole operators, as well as operators with right-handed light-quark fields. In the context of a particular model, all that is needed is to perform a matching calculation determining the Wilson coefficients in the effective Hamiltonian at the weak scale. We find that, quite generally, New Physics contributions would not affect the shape of the photon spectrum, but could change the total branching ratio by a considerable amount. This implies that the analysis of the photon energy and hadronic mass spectra, which is crucial for the experimental determination of the total branching ratio, can be performed without assuming the correctness of the Standard Model. On the other hand, the total branching ratio will provide a powerful constraint on the structure of New Physics beyond the Standard Model, as we have illustrated with some specific examples.

We believe that our work eliminates the remaining elements of model dependence present in previous studies of the photon spectrum in $B \to X_s\gamma$ decays and, therefore, provides a firm theoretical basis for analyses of experimental data on inclusive radiative B decays. We are confident that in the near future, when measurements of the photon spectrum with high statistics will be performed, it will be possible to derive a value for the $B \to X_s\gamma$ branching ratio that is less model-dependent than existing ones, thus providing one of the most sensitive tests of the flavour sector of the Standard Model.

Note added in proof: While this paper was in preparation the CLEO Collaboration presented a preliminary update of the $B \to X_s\gamma$ branching ratio, yielding ${\rm B}(B \to X_s\gamma) = (2.50 \pm 0.47 \pm 0.39) \times 10^{-4}$ [64]. This value has been obtained using the original analysis adopted in [1]. We expect that using our improved theoretical predictions the central value will increase to about 2.8×10^{-4}, which is close to the prediction of the Standard Model.

Acknowledgements. We would like to thank Ahmed Ali, Gerhard Buchalla, Andrzej Buras, Andrzej Czarnecki, Gian Giudice, Laurent Lellouch, Guido Martinelli and Mikolaj Misiak for helpful discussions. We are indebted to Steven Glenn for discussing aspects of the CLEO measurement of the $B \to X_s\gamma$ branching ratio and providing the data on the photon spectrum displayed in Table 4. A.K. was supported by the United States Department of Energy under Grant No. DE-FG02-84ER40153.

Appendix A: QED corrections to $C_7(m_b)$

QED corrections affect the theoretical prediction for the $B \to X_s\gamma$ branching ratio in three ways: there are $O(\alpha)$ matching corrections to the Wilson coefficients $C_i(m_W)$ at the weak scale, there are $O(\alpha)$ contributions to the matrix elements of the operators in the effective Hamiltonian at the scale μ_b, and there are $O(\alpha L)$ corrections to the evolution of the operators from the scale m_W down to the scale μ_b, where $L = \ln(m_W/\mu_b)$. The latter corrections are logarithmically enhanced. They can be accounted for by including the $O(\alpha)$ contributions to the anomalous dimension matrix of the operators in the effective Hamiltonian in the solution of the renormalization-group equation. On the other hand, a complete calculation of the remaining $O(\alpha)$ corrections would be extremely cumbersome. Fortunately, it is likely that these corrections will be smaller than the next-to-next-to-leading QCD corrections of order α_s^2.

When QED corrections are included, as many as twelve operators in the effective Hamiltonian mix under renormalization. Besides the current-current operators O_1 and O_2 and the dipole operators O_7 and O_8, these are four QCD penguin and four electroweak penguin operators. However, it turns out that to a very good approximation the mixing of (O_1, O_2, O_7, O_8) with the penguin operators can be neglected. This approximation reproduces the leading-order results in (9) exactly but for the terms $\sum_i h_i \eta^{a_i}$ and $\sum_i \bar{h}_i \eta^{a_i}$ in $C_7^{(0)}$ and $C_8^{(0)}$. Numerically, $C_7^{(0)}(m_b)$ is reproduced with an accuracy of 3×10^{-3}, and $C_8^{(0)}(m_b)$ with an accuracy of 3.7%.

Including QED corrections, the one-loop anomalous dimension matrix in the truncated operator basis is

$$\boldsymbol{\gamma} = \frac{\alpha_s}{4\pi}\,\boldsymbol{\gamma_0} + \frac{\alpha}{4\pi}\,\boldsymbol{\Gamma_0}\,, \tag{A.1}$$

where

$$\boldsymbol{\gamma_0} = \begin{pmatrix} -2 & 6 & 0 & 3 \\ 6 & -2 & \frac{416}{81} & \frac{70}{27} \\ 0 & 0 & \frac{32}{3} & 0 \\ 0 & 0 & -\frac{32}{9} & \frac{28}{3} \end{pmatrix},$$
$$\boldsymbol{\Gamma_0} = \begin{pmatrix} -\frac{8}{3} & 0 & -\frac{208}{81} & -\frac{8}{27} \\ 0 & -\frac{8}{3} & -\frac{208}{243} & -\frac{116}{81} \\ 0 & 0 & \frac{16}{9} & -\frac{8}{3} \\ 0 & 0 & 0 & \frac{8}{9} \end{pmatrix}. \tag{A.2}$$

We have determined the entries of the QED matrix $\boldsymbol{\Gamma_0}$ using the results of Ciuchini et al. [65] for the contributions to each entry of the QCD matrix $\boldsymbol{\gamma_0}$, taking into account their colour structure and the electric charges of the quark fields involved. We collect the Wilson coefficient functions $C_i^{(0)}$ into a vector $\mathbf{C}$ and write their evolution as

$$\mathbf{C}(\mu) = \mathbf{U}(\mu, m_W)\, \mathbf{C}(m_W)\,, \tag{A.3}$$

where the evolution matrix satisfies the renormalization-group equation

$$\mu \frac{\mathrm{d}}{\mathrm{d}\mu}\, \mathbf{U}(\mu, m_W) = \boldsymbol{\gamma}^T\, \mathbf{U}(\mu, m_W)\,. \tag{A.4}$$

To solve this equation, we make the ansatz

$$\mathbf{U}(\mu, m_W) = \mathbf{K}(\mu)\, \mathbf{U_0}(\mu, m_W)\, \mathbf{K}^{-1}(m_W)\,, \tag{A.5}$$

where $\mathbf{U_0}(\mu, m_W)$ is the leading-order QCD evolution matrix. To first order in the electro-magnetic coupling α we may write

$$\mathbf{K}(\mu) = \mathbf{1} + \alpha \left(\frac{\mathbf{K_0}}{\alpha_s(\mu)} + \ldots \right), \tag{A.6}$$

where the ellipses represent terms that do not contribute at leading-logarithmic order. Inserting this ansatz into the renormalization-group equation satisfied by $\mathbf{K}(\mu)$, we obtain $\mathbf{K_0}$ from the solution of the algebraic equation

$$2\beta_0 \mathbf{K_0} = \boldsymbol{\Gamma_0}^T + [\boldsymbol{\gamma_0}^T, \mathbf{K_0}]\,, \tag{A.7}$$

where $\beta_0 = \frac{23}{3}$ is the first coefficient of the QCD β-function for $n_f = 5$ light quark flavours. Let us introduce the matrix $\mathbf{V}$ that diagonalizes the QCD anomalous dimension matrix, i.e.

$$\mathbf{V}^{-1} \boldsymbol{\gamma_0}^T\, \mathbf{V} \equiv \mathrm{diag}(\gamma_1, \gamma_2, \gamma_3, \gamma_4)\,, \tag{A.8}$$

and denote $\mathbf{k} = \mathbf{V}^{-1} \mathbf{K_0}\, \mathbf{V}$ and $\mathbf{g} = \mathbf{V}^{-1} \boldsymbol{\Gamma_0}^T\, \mathbf{V}$. Then the solution of (A.7) yields

$$k_{ij} = \frac{g_{ij}}{2\beta_0 - (\gamma_i - \gamma_j)}\,. \tag{A.9}$$

The result for the evolution matrix $\mathbf{U}(\mu, m_W)$ can now be written in the form $\mathbf{U}(\mu, m_W) = \mathbf{V}\, \mathbf{u}\, \mathbf{V}^{-1}$, where

$$u_{ij} = \eta_i\, \delta_{ij} + \alpha\, k_{ij} \left(\frac{\eta_i}{\alpha_s(\mu)} - \frac{\eta_j}{\alpha_s(m_W)} \right);$$
$$\eta_i = \left(\frac{\alpha_s(m_W)}{\alpha_s(\mu)} \right)^{\gamma_i/2\beta_0}. \tag{A.10}$$

This general result has previously been derived by Buchalla et al. [66]. The evaluation of this relation for our particular case leads to the expression for the QED coefficient $C_7^{(\mathrm{em})}(\mu_b)$ given in (11). The coefficients of $C_7^{(0)}(m_W)$ and $C_8^{(0)}(m_W)$ in this result are exact, whereas the remaining terms are only approximate because of the truncation of the operator basis. However, as in the case of the QCD evolution we expect that from a numerical point of view the truncation of the basis is justified. Expanding the result (11) to first order in α_s we recover the formula of Czarnecki and Marciano [33]:

$$\frac{\alpha}{\alpha_s(\mu_b)}\, C_7^{(\mathrm{em})}(\mu_b) = \frac{\alpha}{4\pi} \left(\frac{208}{243} - \frac{16}{9}\, C_7^{(0)}(m_W) \right) \times \ln \frac{m_W}{\mu_b} + \ldots\,. \tag{A.11}$$

Numerically, the resummed expression in (11) is smaller than the naive result (A.11) by a factor of about 0.55.

We note that Czarnecki and Marciano also include a particular type of matching correction to the coefficient $C_7(m_W)$ at the weak scale, arising from fermion-loop insertions on the W-propagator in the top-quark–W penguin diagram [33]. The resulting contribution is $\Delta C_7(m_W) \approx 0.53\alpha$, which at the scale m_b yields a contribution $\Delta C_7(m_b) \approx 0.36\alpha \approx 2.6 \times 10^{-3}$. Since there are many other matching corrections that have not yet been calculated, and since there are similar $O(\alpha)$ contributions to the matrix elements of the local operators O_i that are neglected, we see no compelling reason to include this particular matching contribution. Its effect on the total branching ratio does not exceed the level of 1% and is thus safely within the theoretical uncertainty of $\pm 2\%$, which we assign to higher-order electroweak corrections.

Appendix B: Photon spectrum in decays of B mesons produced at the $\Upsilon(4s)$ resonance

We denote by E_γ^{lab} the photon energy measured in the laboratory, and by E_γ the one measured in the B rest frame. If $\mathrm{dB}/\mathrm{d}E_\gamma$ is the photon spectrum in the B rest frame, the corresponding spectrum measured in the laboratory is

$$\frac{\mathrm{dB}}{\mathrm{d}E_\gamma^{\mathrm{lab}}} = \frac{1}{\beta_+ - \beta_-} \int\limits_{\beta_- E_\gamma^{\mathrm{lab}}}^{E_1(E_\gamma^{\mathrm{lab}})} \mathrm{d}E_\gamma\, \frac{1}{E_\gamma}\, \frac{\mathrm{dB}}{\mathrm{d}E_\gamma}\,, \tag{B.1}$$

where

$$\beta_\pm = \sqrt{\frac{1 \pm \beta}{1 \mp \beta}} \approx 1 \pm \beta\,,$$
$$E_1(E_\gamma^{\mathrm{lab}}) = \min(\beta_+ E_\gamma^{\mathrm{lab}}, E_\gamma^{\max})\,. \tag{B.2}$$

The maximum photon energy in the laboratory is $(E_\gamma^{\mathrm{lab}})_{\max} = \beta_+ E_\gamma^{\max}$.

It is straightforward to calculate from (B.1) the effect of the boost on the partially integrated branching ratio. Let us define the difference

$$\Delta(E_0) = \int\limits_{E_0}^{(E_\gamma^{\rm lab})_{\rm max}} {\rm d}E_\gamma^{\rm lab}\, \frac{{\rm dB}}{{\rm d}E_\gamma^{\rm lab}} - \int\limits_{E_0}^{E_\gamma^{\rm max}} {\rm d}E_\gamma\, \frac{{\rm dB}}{{\rm d}E_\gamma}\,. \quad \text{(B.3)}$$

Then, provided that $E_0 < \beta_- E_\gamma^{\rm max}$, we find that

$$\begin{aligned}\Delta(E_0) &= \frac{1-\beta}{2\beta} \int\limits_{E_0}^{\beta_+ E_0} {\rm d}E_\gamma\, \frac{{\rm dB}}{{\rm d}E_\gamma} \left(1 - \frac{\beta_+ E_0}{E_\gamma}\right) \\ &\quad + \frac{1+\beta}{2\beta} \int\limits_{\beta_- E_0}^{E_0} {\rm d}E_\gamma\, \frac{{\rm dB}}{{\rm d}E_\gamma} \left(1 - \frac{\beta_- E_0}{E_\gamma}\right) \\ &= -\frac{\beta^2 E_0^3}{6} \left(\frac{\rm d}{{\rm d}E}\, \frac{1}{E}\, \frac{{\rm dB}}{{\rm d}E}\right)_{E=E_0} + O(\beta^4)\,, \end{aligned} \quad \text{(B.4)}$$

i.e. the effect is quadratic in the small quantity β. With $E_0 = 2.2\,{\rm GeV}$ as in the CLEO analysis, we find that $\Delta(E_0) \approx -(0.04\text{–}0.09) \times 10^{-4}$ depending on the parameters of the shape function, which is a very small effect.

Appendix C: Results for the functions $s_{ij}(y)$ and $d_{ij}(\delta)$

The functions $s_{ij}(y)$ entering the theoretical expressions for the photon spectrum are given by the derivatives of the functions $f_{ij}(\delta)$ in (16) through $s_{ij}(y) = f'_{ij}(1-y)$. Explicitly, we find

$$\begin{aligned} s_{77}(y) &= \frac{1}{3}\left[7 + y - 2y^2 - 2(1+y)\ln(1-y)\right], \\ s_{88}(y) &= \frac{1}{27}\left\{\frac{2(2-2y+y^2)}{y}\left[\ln(1-y) + 2\ln\frac{m_b}{m_s}\right]\right. \\ &\quad \left. -2y^2 - y - \frac{8(1-y)}{y}\right\}, \\ s_{78}(y) &= \frac{8}{9}\left[\frac{1-y}{y}\ln(1-y) + 1 + \frac{y^2}{4}\right], \\ s_{22}(y) &= \frac{16}{27}\int\limits_0^y {\rm d}x\,(1-x)\left|\frac{z}{x}\,G\Big(\frac{x}{z}\Big) + \frac{1}{2}\right|^2, \\ s_{27}(y) &= -3s_{28}(y) = -\frac{8z}{9}\int\limits_0^y {\rm d}x\,{\rm Re}\Big[G\Big(\frac{x}{z}\Big) + \frac{x}{2z}\Big]. \end{aligned} \quad \text{(C.1)}$$

The functions $d_{ij}(\delta)$ entering the expression for the average photon energy in (37) are given by

$$d_{ij}(\delta) = \int\limits_0^\delta {\rm d}x\, f_{ij}(x) - \delta\, f_{ij}(\delta)\,. \quad \text{(C.2)}$$

We find

$$\begin{aligned} d_{77}(\delta) &= \frac{2\delta^2}{9}(3-\delta)\ln\delta - \frac{4\delta^2}{3} - \frac{7\delta^3}{27} + \frac{\delta^4}{6}, \\ d_{88}(\delta) &= \frac{8}{27}\left(\ln\frac{m_b}{m_s} - 1\right)\left[\ln(1-\delta) + \delta + \frac{\delta^2}{4} + \frac{\delta^3}{6}\right] \\ &\quad + \frac{4}{27}\left[\frac{\pi^2}{6} - L_2(1-\delta) + \left(\delta + \frac{\delta^2}{4} + \frac{\delta^3}{6}\right)\ln\delta\right. \\ &\quad \left. -\delta - \frac{\delta^2}{4} - \frac{5\delta^3}{36} + \frac{\delta^4}{8}\right], \\ d_{78}(\delta) &= \frac{8}{9}\left[\frac{\pi^2}{6} - L_2(1-\delta) + \left(\delta + \frac{\delta^2}{2}\right)\ln\delta\right. \\ &\quad \left. -\delta - \frac{7\delta^2}{8} + \frac{\delta^3}{6} - \frac{\delta^4}{16}\right], \\ d_{22}(\delta) &= -\frac{8}{27}\int\limits_0^1 {\rm d}x\,(1-x)(1-x_\delta)^2\left|\frac{z}{x}\,G\Big(\frac{x}{z}\Big) + \frac{1}{2}\right|^2, \\ d_{27}(\delta) &= -3d_{28}(\delta) \\ &= \frac{4z}{9}\int\limits_0^1 {\rm d}x\,(1-x_\delta)^2\,{\rm Re}\Big[G\Big(\frac{x}{z}\Big) + \frac{x}{2z}\Big]. \end{aligned} \quad \text{(C.3)}$$

The function $\bar{d}_{77}(\delta)$ is defined as

$$\bar{d}_{77}(\delta) = d_{77}(\delta) + \delta\left(1 + \frac{4}{3}\ln\delta\right) + \frac{23}{54}\,. \quad \text{(C.4)}$$

The second term is the contribution of the Sudakov logarithms. It is this contributions which, in large orders, develops a factorial divergence that cancels the infrared renormalon of the pole mass [42]. The last term in (C.4) is adjusted such that $\bar{d}_{77}(1) = 0$. This condition defines the coefficient $C_E[\alpha_s]$ in (37).

References

1. M.S. Alam et al. (CLEO Collaboration), Phys. Rev. Lett. **74**, 2885 (1995)
2. R. Barate et al. (ALEPH Collaboration), Phys. Lett. B **429**, 169 (1998)
3. J. Chay, H. Georgi, B. Grinstein, Phys. Lett. B **247**, 399 (1990)
4. I.I. Bigi, N.G. Uraltsev, A.I. Vainshtein, Phys. Lett. B **293**, 430 (1992) [E: **297**, 477 (1993)]; I.I. Bigi, M.A. Shifman, N.G. Uraltsev, A.I. Vainshtein, Phys. Rev. Lett. **71**, 496 (1993); B. Blok, L. Koyrakh, M.A. Shifman, A.I. Vainshtein, Phys. Rev. D **49**, 3356 (1994) [E: **50**, 3572 (1994)]
5. A.V. Manohar, M.B. Wise, Phys. Rev. D **49**, 1310 (1994)
6. A.F. Falk, M. Luke, M.J. Savage, Phys. Rev. D **49**, 3367 (1994)
7. M.B. Voloshin, Phys. Lett. B **397**, 275 (1997)
8. A. Khodjamirian, R. Rückl, G. Stoll, D. Wyler, Phys. Lett. B **402**, 167 (1997)
9. Z. Ligeti, L. Randall, M.B. Wise, Phys. Lett. B **402**, 178 (1997)
10. A.K. Grant, A.G. Morgan, S. Nussinov, R.D. Peccei, Phys. Rev. D **56**, 3151 (1997)

11. G. Buchalla, G. Isidori, S.J. Rey, Nucl. Phys. B **511**, 594 (1998)
12. B. Grinstein, R. Springer, M.B. Wise, Nucl. Phys. B **339**, 269 (1990)
13. M. Ciuchini et al., Phys. Lett. B **316**, 127 (1993)
14. A.J. Buras, M. Misiak, M. Münz, S. Pokorski, Nucl. Phys. B **424**, 374 (1994)
15. K. Adel, Y.P. Yao, Phys. Rev. D **49**, 4945 (1994)
16. C. Greub, T. Hurth, Phys. Rev. D **56**, 2934 (1997)
17. A. Ali, C. Greub, Phys. Lett. B **361**, 146 (1995); see also the extended version in Preprint DESY 95-117 [hep-ph/9506374]
18. C. Greub, T. Hurth, D. Wyler, Phys. Lett. B **380**, 385 (1996); Phys. Rev. D **54**, 3350 (1996)
19. K. Chetyrkin, M. Misiak, M. Münz, Phys. Lett. B **400**, 206 (1997) [E: **425**, 414 (1998)]
20. A.J. Buras, A. Kwiatkowski, N. Pott, Phys. Lett. B **414**, 157 (1997)
21. M. Ciuchini, G. Degrassi, P. Gambino, G.F. Giudice, Nucl. Phys. B **527**, 21 (1998)
22. F.M. Borzumati, C. Greub, Preprint ZU-TH-31-97 [hep-ph/9802391]
23. S. Glenn, private communication
24. A. Ali, C. Greub, Phys. Lett. B **259**, 182 (1991)
25. G. Altarelli et al., Nucl. Phys. B **208**, 365 (1982)
26. M. Neubert, Phys. Rev. D **49**, 3392 and 4623 (1994)
27. I.I. Bigi, M.A. Shifman, N.G. Uraltsev, A.I. Vainshtein, Int. J. Mod. Phys. A **9**, 2467 (1994); R.D. Dikeman, M. Shifman, N.G. Uraltsev, Int. J. Mod. Phys. A **11**, 571 (1996)
28. T. Mannel, M. Neubert, Phys. Rev. D **50**, 2037 (1994)
29. This point has also been emphasized in: A.F. Falk, Preprint JHU-TIPAC-97023 [hep-ph/9712364], to appear in the Proceedings of Beauty '97, Los Angeles, California, October 1997
30. M. Gronau, D. London, Phys. Rev. D **55**, 2845 (1997)
31. J.L. Hewett, Preprint SLAC-PUB-7774 [hep-ph/9803370]
32. For a review, see: G. Buchalla, A.J. Buras, M.E. Lautenbacher, Rev. Mod. Phys. **68**, 1125 (1996)
33. A. Czarnecki, W.J. Marciano, Phys. Rev. Lett. **81**, 277 (1998)
34. P. Drell, Preprint CLNS-97-1521 [hep-ex/9711020], to appear in the *Proceedings of the 18th International Symposium on Lepton–Photon Interactions*, Hamburg, Germany, July 1997
35. M. Neubert, Preprint CERN-TH/98-2 [hep-ph/9801269], to appear in the *Proceedings of the International Europhysics Conference on High Energy Physics*, Jerusalem, Israel, August 1997
36. A. Sirlin, Nucl. Phys. B **196**, 83 (1982)
37. Y. Nir, Phys. Lett. B **221**, 184 (1989)
38. A. Kapustin, Z. Ligeti, H.D. Politzer, Phys. Lett. B **357**, 653 (1995)
39. A.F. Falk, M. Neubert, Phys. Rev. D **47**, 2965 (1993)
40. G.P. Korchemsky, G. Sterman, Phys. Lett. B **340**, 96 (1994)
41. R. Akhoury, I.Z. Rothstein, Phys. Rev. D **54**, 2349 (1996)
42. M. Neubert, Preprint CERN-TH/98-126, in preparation
43. A.J. Buras, Proceedings of the 28th International Conference on High-Energy Physics, Warsaw, Poland, July 1996, edited by Z. Ajduk, A.K. Wroblewski (World Scientific, Singapore, 1997), pp. 243
44. A.L. Kagan, M. Neubert, Preprint CERN-TH/98-1 [hep-ph/9803368]
45. A. Kapustin, Z. Ligeti, Phys. Lett. B **355**, 318 (1995)
46. C. Bauer, Phys. Rev. D **57**, 5611 (1998)
47. M. Beneke, V.M. Braun, Nucl. Phys. B **426**, 301 (1994)
48. I.I. Bigi, M.A. Shifman, N.G. Uraltsev, A.I. Vainshtein, Phys. Rev. D **50**, 2234 (1994)
49. E.C. Poggio, H.R. Quinn, S. Weinberg, Phys. Rev. D **13**, 1958 (1976)
50. R.M. Barnett et al. (Particle Data Group), Phys. Rev. D **54**, 1 (1996)
51. R. Ammar et al. (CLEO Collaboration), Phys. Rev. Lett. **71**, 674 (1993)
52. A. Ali, G.F. Giudice, T. Mannel, Z. Phys. C **67**, 417 (1995)
53. J.L. Hewett, J.D. Wells, Phys. Rev. D **55**, 5549 (1997)
54. A.L. Kagan, Phys. Rev. D **51**, 6196 (1995)
55. B.G. Grzadkowski, W.-S. Hou, Phys. Lett. B **272**, 383 (1991)
56. M. Ciuchini, E. Gabrielli, G.F. Giudice, Phys. Lett. B **388**, 353 (1996) [E: **393**, 489 (1997)]
57. A.L. Kagan, J. Rathsman, Preprint [hep-ph/9701300]; A.L. Kagan, *Proceedings of the 2nd International Conference on B Physics and CP Violation*, Honolulu, Hawaii, March 1997, edited by T.E. Browder et al. (World Scientific, Singapore, 1998), p. 510
58. A.L. Kagan, Preprint UCTP-107-98 [hep-ph/9806266], to appear in the *Proceedings of the 7th International Symposium on Heavy Flavor Physics*, Santa Barbara, California, July 1997
59. T.E. Coan et al. (CLEO Collaboration), Phys. Rev. Lett. **80**, 1150 (1998)
60. A.L. Kagan, *Proceedings of the 15th Johns Hopkins Workshop on Current Problems in Particle Theory*, Baltimore, Madison, August 1991, edited by G. Domokos, S. Kovesi-Domokos (World Scientific, Singapore, 1992), pp. 217
61. B.A. Dobrescu, Nucl. Phys. B **449**, 462 (1995); B.A. Dobrescu, J. Terning, Phys. Lett. B **416**, 129 (1998)
62. G.L. Kane, C. Kolda, L. Roszkowski, J.D. Wells, Phys. Rev. D **49**, 6173 (1994)
63. T.G. Rizzo, Phys. Rev. D **58**, 05009 (1998)
64. S. Glenn (representing the CLEO Collaboration), talk presented at the Meeting of the American Physics Society, Columbus, Ohio, 18–21 March 1998
65. M. Ciuchini, E. Franco, L. Reina, L. Silvestrini, Nucl. Phys. B **421**, 41 (1994)
66. G. Buchalla, A.J. Buras, M.K. Harlander, Nucl. Phys. B **337**, 313 (1990)